Results in Chemistry

COUNTRY

Netherlands

Universities and research institutions in Netherlands

Media Ranking in Netherlands

SUBJECT AREA AND CATEGORY

Chemistry
Chemistry (miscellaneous)

PUBLISHER

Elsevier B.V.

SJR 2024

0.605 Q2

H- INDEX

33

PUBLICATION TYPE

Journals

ISSN

22117156

COVERAGE

2019-2025

INFORMATION

Homepage

How to publish in this journal

SCOPE

Results in Chemistry is an open access journal, indexed in Scopus, offering authors the opportunity to publish in all fundamental and interdisciplinary areas of chemistry and related fields. Papers of experimental, theoretical and computational nature are all welcome. Results in Chemistry accepts papers that are scientifically sound, technically correct and provide valuable new knowledge to the chemistry community. Results in Chemistry welcomes four types of papers: Full research papers Review articles Communications (up to 3500 words) Microarticles: very short papers, no longer than 2-3 pages. They may consist of a single, but well-described piece of information, such as: - Data and/or a plot plus a description - Description of a new method or instrumentation - Concept or design study - Code

FIND SIMILAR JOURNALS

option:

1	2	3	4	5
Asian Journal of Chemistry	Journal of Saudi Chemical Society	ChemistrySelect	Journal of the Iranian Chemical Society	Journal of Chemical Research
IND	NLD	GBR	DEU	GBR
84% similarity	83% similarity	77% similarity	76% similarity	72% similarity

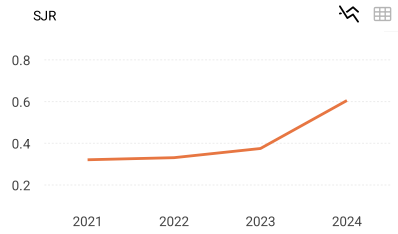

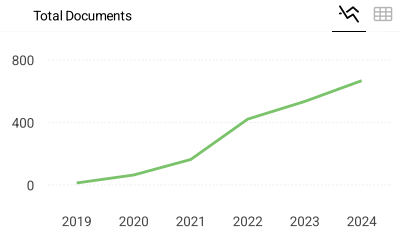

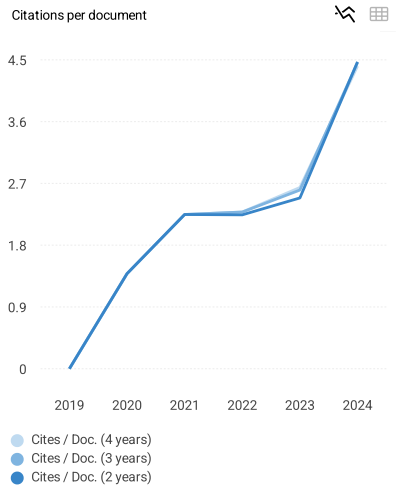

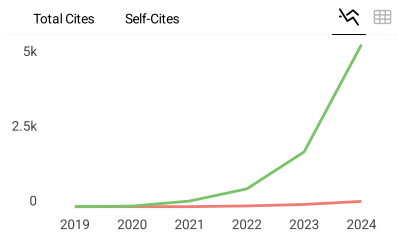

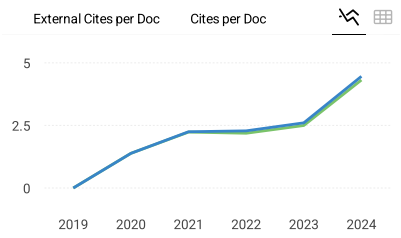

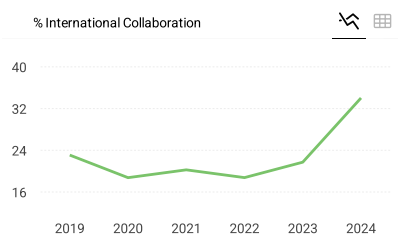

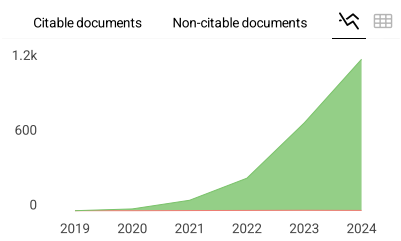

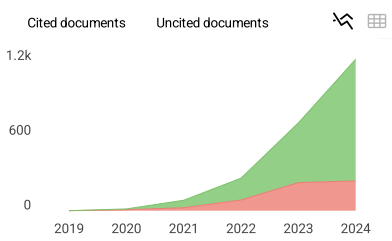

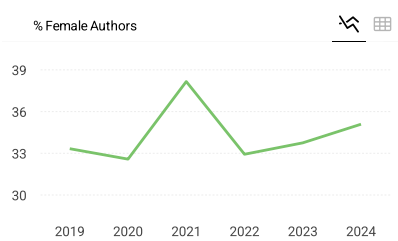

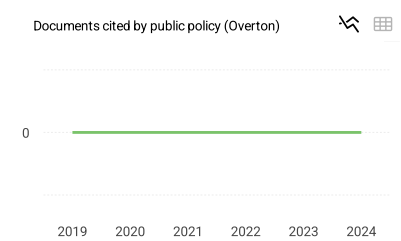

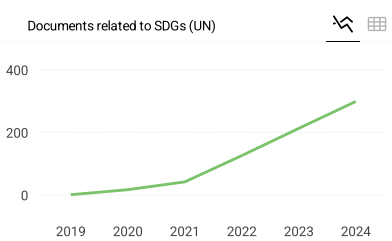

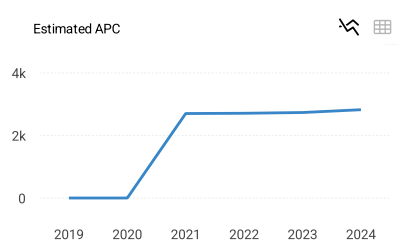

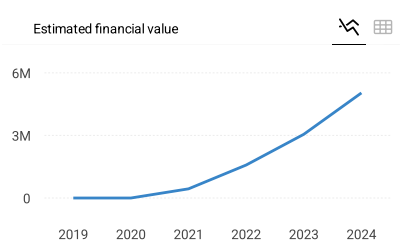

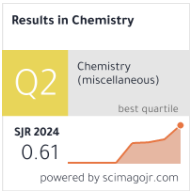

← Show this widget in your own website

Just copy the code below and paste within your html code:

<a href="https://www.scimag

SCImago Graphica

Explore, visually communicate and make sense of data with our new data visualization tool.

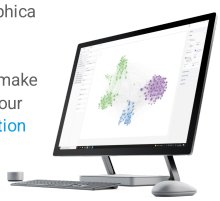

Close

Results in Chemistry

Open access

4.8 CiteScore

2.5 Impact Factor

About the journal

Results in Chemistry is an open access journal, indexed in Scopus with an Impact Factor, offering authors the opportunity to publish in all fundamental and interdisciplinary areas of chemistry and related fields. Papers of experimental, theoretical and computational nature are all welcome. *Results* ...

View full aims & scope

Article publishing option

Open Access

Article Publishing Charge (APC): **USD 1,740 (excluding taxes).**
This journal is taking part in the GPOA pilot.
Review this journal's open access policy.

26 days
Time to first decision

58 days
Review time

64 days
Submission to acceptance

8 days
Acceptance to publication

View all insights

Editor-in-Chief | View full editorial board

Thorfinnur Gunnlaugsson, PhD

Trinity College Dublin School of Chemistry, Dublin, Ireland

Articles

efine Your Search Results

Results in Chemistry

Search

rt By: Relevancy

Filters

Clear All

Web of Science Coverage

Core Collection

- [x] Science Citation Index Expanded (SCIE)
- [x] Social Sciences Citation Index (SSCI)
- [x] Arts & Humanities Citation Index (AHCI)
- [x] Emerging Sources Citation Index (ESCI)

Current Contents

- [ ] Agriculture, Biology & Environmental Sciences
- [ ] Arts & Humanities
- [ ] Business Collection
- [ ] Clinical Medicine
- [ ] Electronics & Telecommunications Collection
- [ ] Engineering, Computing & Technology
- [ ] Life Sciences
- [ ] Physical, Chemical & Earth Sciences
- [ ] Social And Behavioral Sciences

Other

- [ ] BIOSIS
- [ ] Current Chemical Reactions
- [ ] Essential Science Indicators
- [ ] Index Chemicus

tive Filters

SCIENCE CITATION INDEX EXPANDED (SCIE) × SOCIAL SCIENCES CITATION INDEX (SSCI) ×

ARTS & HUMANITIES CITATION INDEX (AHCI) × EMERGING SOURCES CITATION INDEX (ESCI) ×

earch Results

und 1,161 results (Page 1) Share These Results

xact Match Found

RESULTS IN CHEMISTRY

OPEN ACCESS

Publisher: ELSEVIER , RADARWEG 29, AMSTERDAM, Netherlands, 1043 NX

ISSN / eISSN: 2211-7156

Web of Science Core Collection: Emerging Sources Citation Index

Share This Journal View profile page

** Requires free login.*

ther Possible Matches

ACS EARTH AND SPACE CHEMISTRY

Publisher: AMER CHEMICAL SOC , 1155 16TH ST, NW, WASHINGTON, USA, DC, 20036

ISSN / eISSN: 2472-3452

Web of Science Core Collection: Science Citation Index Expanded

Additional *Web of Science* Indexes: Current Contents Physical, Chemical & Earth Sciences | Essential Science Indicators

Share This Journal View profile page

** Requires free login.*

ACS MEDICINAL CHEMISTRY LETTERS

Publisher: AMER CHEMICAL SOC , 1155 16TH ST, NW, WASHINGTON, USA, DC, 20036

ISSN / eISSN: 1948-5875

Web of Science Core Collection: Science Citation Index Expanded

Additional *Web of Science* Indexes: Biological Abstracts | BIOSIS Previews | Current Chemical Reactions | Current Contents Life Sciences | Essential Science Indicators | Index Chemicus

Share This Journal View profile page

Zoological Record

Open Access

Category

Country / Region

Language

Frequency

Journal Citation Reports

* Requires free login.

ACS PHYSICAL CHEMISTRY AU

OPEN ACCESS

Publisher: AMER CHEMICAL SOC , 1155 16TH ST, NW, WASHINGTON, USA, DC, 20036

ISSN / eISSN: 2694-2445

Web of Science Core Collection: Emerging Sources Citation Index

Share This Journal

View profile page

* Requires free login.

ACS SUSTAINABLE CHEMISTRY & ENGINEERING

Publisher: AMER CHEMICAL SOC , 1155 16TH ST, NW, WASHINGTON, USA, DC, 20036

ISSN / eISSN: 2168-0485

Web of Science Core Collection: Science Citation Index Expanded

Additional *Web of Science* Indexes: Current Contents Engineering, Computing & Technology | Current Contents Physical, Chemical & Earth Sciences | Essential Science Indicators

Share This Journal

View profile page

* Requires free login.

ACTA CRYSTALLOGRAPHICA SECTION C-STRUCTURAL CHEMISTRY

Publisher: INT UNION CRYSTALLOGRAPHY , 2 ABBEY SQ, CHESTER, ENGLAND, CH1 2HU

ISSN / eISSN: 2053-2296

Web of Science Core Collection: Science Citation Index Expanded

Additional *Web of Science* Indexes: Current Contents Physical, Chemical & Earth Sciences | Essential Science Indicators

Share This Journal

View profile page

* Requires free login.

ANALYTICAL AND BIOANALYTICAL CHEMISTRY

Publisher: SPRINGER HEIDELBERG , TIERGARTENSTRASSE 17, HEIDELBERG, GERMANY, D-69121

ISSN / eISSN: 1618-2642 / 1618-2650

Web of Science Core Collection: Science Citation Index Expanded

Additional *Web of Science* Indexes: Biological Abstracts | BIOSIS Previews | Current Contents Physical, Chemical & Earth Sciences | Essential Science Indicators

Share This Journal

View profile page

* Requires free login.

ANALYTICAL AND BIOANALYTICAL CHEMISTRY RESEARCH

Publisher: IRANIAN CHEMICAL SOC , NO 7, MARAGHEH ST, OSTAD NEJATOLLAHI AVE, PO BOX 15875-1169, TEHRAN, IRAN, 00000

ISSN / eISSN: 2383-093X

Web of Science Core Collection: Emerging Sources Citation Index

Share This Journal View profile page

** Requires free login.*

ANALYTICAL CHEMISTRY

Publisher: **AMER CHEMICAL SOC , 1155 16TH ST, NW, WASHINGTON, USA, DC, 20036**

ISSN / eISSN: **0003-2700 / 1520-6882**

Web of Science Core Collection: **Science Citation Index Expanded**

Additional *Web of Science* Indexes: **Current Contents Life Sciences | Current Contents Physical, Chemical & Earth Sciences | Essential Science Indicators**

Share This Journal View profile page

** Requires free login.*

ANALYTICAL CHEMISTRY LETTERS

Publisher: **TAYLOR & FRANCIS LTD , 2-4 PARK SQUARE, MILTON PARK, ABINGDON, England, OXON, OX14 4RN**

ISSN / eISSN: **2229-7928 / 2230-7532**

Web of Science Core Collection: **Emerging Sources Citation Index**

Share This Journal View profile page

** Requires free login.*

Items per page: 10 1 – 10 of 1161


Results in
Chemistry

Volume 3

January 2021

Previous vol/issue

Next vol/issue

Receive an update when the latest issues in this journal are published

Sign in to set up alerts

Open access

Editorial Board

Article 100267

View PDF

VSI:Dyes, probes and Results

Research article *Open access*

One-step condensation synthesis and characterizations of indocyanine green

Xiangning Fang, Wenjuan Liu, Xia Wu, Wei Zhou, ... Zhaochao Xu

Article 100092

View PDF Article preview

Abstract Graphical abstract

Graphical abstract

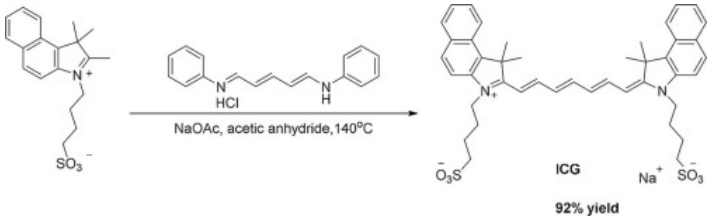

View PDF Article preview

Abstract Graphical abstract

Graphical abstract

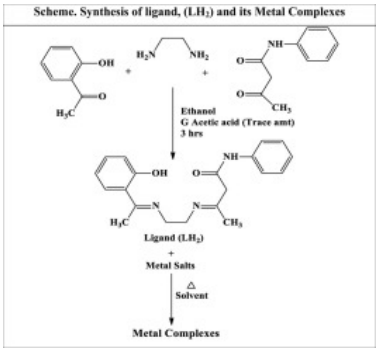

Research article *Open access*

Photoactivatable 1,2-dioxetane chemiluminophores

Lucas S. Ryan, Andrew Nakatsuka, Alexander R. Lippert

Article 100106

View PDF Article preview

Abstract Graphical abstract

Graphical abstract

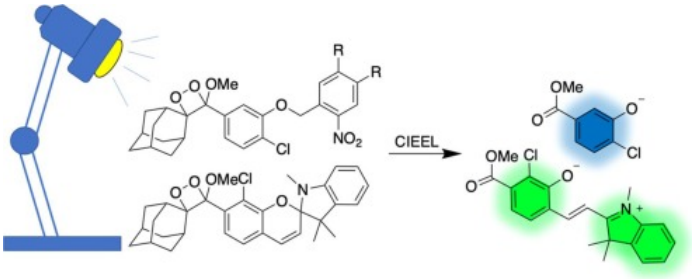

Analytical Chemistry

Research article *Open access*

Turn on fluorescence sensor for specific detection of glycoligand-receptor recognitions based graphene oxide nanocomposite

Faqiong Ou, Zhenmei Lin, Li Li, Yaoping Tang, Ziqian Zhang

Article 100140

View PDF Article preview

Abstract Graphical abstract

Graphical abstract

Research article *Open access*

Naphthalimide-based probe with strong two-photon excited fluorescence and high specificity to cell membranes

Xiaoli Zhang, Huizi Man, Yi Xiao

Article 100100

View PDF Article preview

Abstract Graphical abstract

Graphical abstract

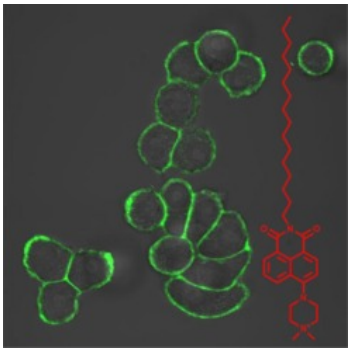

Research article *Open access*

Environment-insensitive two-photon ratiometric probe for *in cellulo* quantitative measurement of hydrogen peroxide

Seo Won Cho, Yong Woong Jun, Ye Jin Reo, Sourav Sarkar, Kyo Han Ahn

Article 100117

View PDF Article preview

Abstract Graphical abstract

Graphical abstract

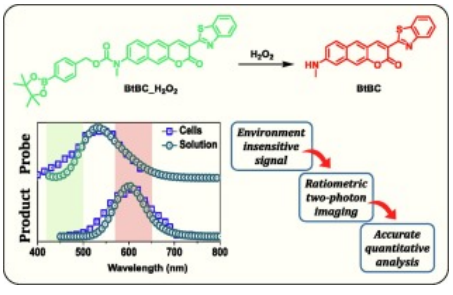

Physical Chemistry and Chemical Physics

Research article *Open access*

Detection of benzo[a]pyrene with silver nanorod substrate in river water and soil based on surface-enhanced raman scattering

Wenxi Cao, Ying Luo, Jingwen Li, Anyi Qian, ... Caiqin Han

Article 100126

nanorod (AgNR) substrate was developed for detecting BaP in river water and soil. Vibration modes of BaP's characteristic peaks were calculated by density functional theory (DFT). The characteristic peak of BaP is at 1234cm^{-1}. In the range of 10~100ppb, the characteristic peak intensity of BaP shows good linear relationship with the concentration. The limit of detection (LOD) is down to 1ppm in river water and 10ppm in soil, respectively. These results demonstrate the applicability of the AgNR substrate for SERS detection of BaP which present an application prospect of AgNR substrate in environmental detection.

Theoretical and Computational Chemistry

Research article *Open access*

Theoretical studies on triplet formations in nitrobenzoxadiazole (NBD) derivatives: The impact of donor group and heteroatom substitution

Chao Wang, Hui Juan Koh, Zhaochao Xu, Xiaogang Liu

Article 100116

View PDF Article preview

Abstract Graphical abstract

Graphical abstract

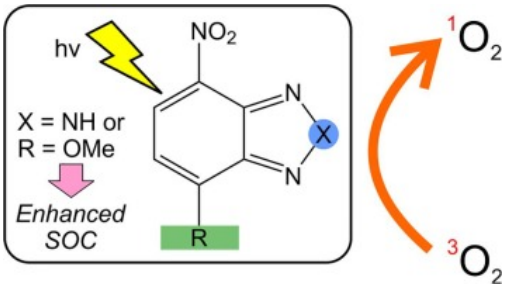

Medicinal Chemistry and Chemical Biology

Review article *Open access*

Triazole, imidazole, and thiazole-based compounds as potential agents against coronavirus

Insa Seck, Filomain Nguemo

Article 100132

View PDF Article preview

Abstract

Abstract

The expansion of the novel coronavirus known as SARS-CoV-2 (severe acute respiratory syndrome coronavirus 2), COVID-19 (coronavirus disease 2019), or 2019-nCoV (2019 novel coronavirus) is a global concern over its pandemic potential. The need for therapeutic alternatives to stop this new pandemic is urgent. Nowadays, no efficacious therapy is available, and vaccines and drugs are underdeveloped to cure or prevent SARS-CoV-2 infections in many countries. Some vaccines candidates have been approved; however, a number of people are still skeptical of this coronavirus vaccines. Probably because of issues related to the quantity of the vaccine and a possible long-term side effects which are still being studied. The previous pandemics of infections caused by coronavirus, such as SARS-CoV in 2003, the Middle East respiratory syndrome coronavirus (MERS-CoV) in 2012, HCoV-229E, and HCoV-OC43 were described in the 1960s, -HCoV-NL63 isolated in 2004, and HCoV-HKU1identified in 2005 prompted

View PDF Article preview

Abstract

Abstract

Fluorescence-based in vitro assays are highly sensitive, selective and convenient to use, which is suitable for qualitative and quantitative detection of various types of biological samples. Herein, we designed and synthesized a novel fluorogenic probe **TPAN-Asn** for in vitro L-asparaginase detection. **TPAN-Asn** exhibited selective and robust response to L-asparaginase over various anions, cations and amino acids. More importantly, we have demonstrated that **TPAN-Asn** is able to accurately quantify the amount of L-asparaginase in patient serum samples. These results suggest that **TPAN-Asn** holds great potential in the benchmarking and analysis of L-asparaginase-based cancer therapy.

Research article *Open access*

Fluorogenic probes for thioredoxin reductase activity

Tendai J. Mafireyi, Jorge O. Escobedo, Robert M. Strongin

Article 100127

View PDF Article preview

Abstract Graphical abstract

Graphical abstract

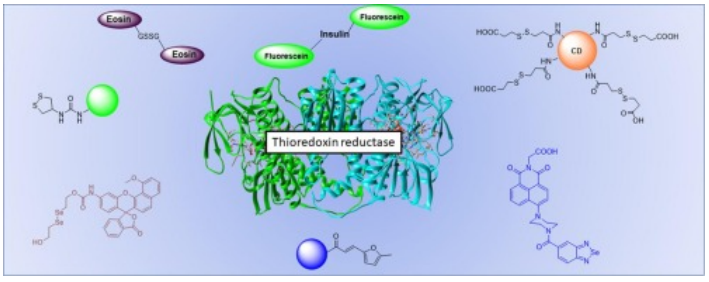

Others

Research article *Open access*

Fluorescent 4-amino-1,8-naphthalimide Tröger's bases possessing conjugated 4-amino-1,8-naphthalimide moieties and their potential fullerenes Host-Guest complexes

Samantha A. Murphy, Oxana Kotova, Steve Comby, Thorfinnur Gunnlaugsson

Article 100128

View PDF Article preview

Abstract Graphical abstract

Graphical abstract

Organic Chemistry

Research article *Open access*

Unanticipated ionic ferrocenyl compounds based on 5,5′-bis(1-hydroxytetrazole). Molecular structures, anti-migration and burning rate catalytic performances

Fangfang Xing, Xiaoling Shi, Fuqiang Bi, Jizhen Li, Guofang Zhang

Article 100090

View PDF Article preview

Abstract Graphical abstract

Graphical abstract

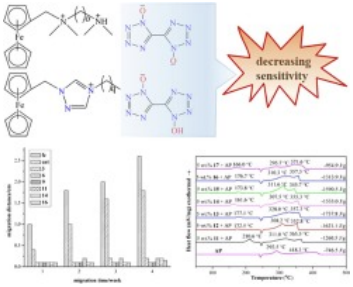

Research article *Open access*

NMR spectroscopic investigation of benzothiazolylacetonitrile azo dyes: CR7 substitution effect and semiempirical study

H.M. Alsoghier, M. Abdellah, H.M. Rageh, H.M.A. Salman, ... S.A. Ibrahim

Article 100088

View PDF Article preview

Abstract

Abstract

Ebead et al. had reported in the synthesis and the UV–Visible solvatochromism combined with semiempirical calculations to study the tautomerism of 1,3-benzothiazol-2-ylacetonitrile azo dyes [1]. In this study, 1,3-benzothiazol-2-ylacetonitrile azo dyes (**1**–**6**) have been resynthesized, one and two dimensional ^{1}H and ^{13}C NMR, as well as absorption and emission spectra, were collected and interpreted. The obtained results were used to clarify the tautomerization phenomenon of these dyes. Predominantly, these dyes exist in *Z*-hydrazone form reinforced through intramolecular hydrogen bonding in deuterated chloroform. Substituents (**R**) in carbon**7** (**CR7**) are the key player of the changes in ^{1}H and ^{13}C NMR chemical shifts, also in the absorption and emission wavelengths of benzothiazole azo dyes. Also, the relative photoluminescence quantum yields (PL QY) of these dyes (**1**–**6**) were estimated and related to the nature of substituents. Finally, PM6 semiempirical calculations were employed to confirm the preferred geometric structure and experimental NMR, absorption, and emission results.

Research article *Open access*

Synthesis of novel coumarin-thiazolidine-2,4-dione derivatives: An approach to computational studies and biological evaluation

Sumitra N. Mangasuli

Article 100105

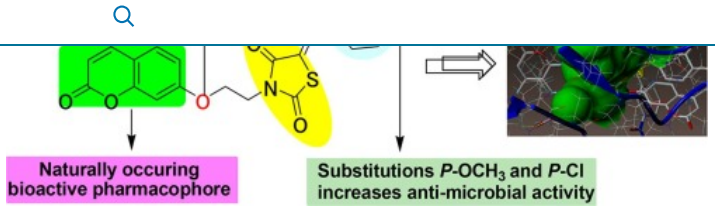

Research article *Open access*

Determination of SADT and TMRad of 3-bromo-1-(3,5-dichloropyridin-2-yl)-4,5-dihydro-1*H*-pyrazole-5-carboxylic acid: Applying thermal decomposition kinetics

Yun-Bo Cong, Zhen-Yun Wei, Xiao-Hua Ma, Zi-Liang Li, ... Chun-Sheng Cheng

Article 100112

View PDF Article preview

Abstract

Abstract

The aim of this study was the evaluation of the safety parameters: Time to Maximum Rate under adiabatic conditions (TMR_{ad}) and self-accelerating decomposition temperature (SADT) for 3-bromo-1-(3,5-dichloropyridin-2-yl)-4,5-dihydro-1*H*-pyrazole −5-carboxylic acid (BDPCA) using evaluated kinetic parameters. The required decomposition kinetics was determined from the results of differential scanning calorimetry (DSC), microcalorimetry (C600), and adiabatic accelerating calorimeter (ARC). AKTS Thermokinetics (TK) and Thermal Safety (TS) Software were used for evaluation of the kinetic parameters of a decomposition reaction. The kinetic analysis was based on the isoconversional Friedman method. The values of TMR_{ad} amount to 110.2 °C, 107.3 °C, and 104.9 °C when calculated from the data collected by DSC, C600, and ARC, respectively. The simulated values of SADT for a 50 kg package of BDPCA amount to 101 °C and 96 °C when elaborating the DSC and C600 signals, respectively. Obtained results indicate that the application of kinetic parameters evaluated from the experiments carried out by three different calorimetric devices resulted in the evaluation of consistent safety parameters.

Research article *Open access*

Visible-light-driven reductive coupling of aromatic ketones using perylene derivatives as photoredox catalysts: Improvement of reaction efficiency by the addition of acetic acid

Hiroyuki Ito, Atsushi Sudo

Article 100123

View PDF Article preview

Abstract Graphical abstract

Graphical abstract

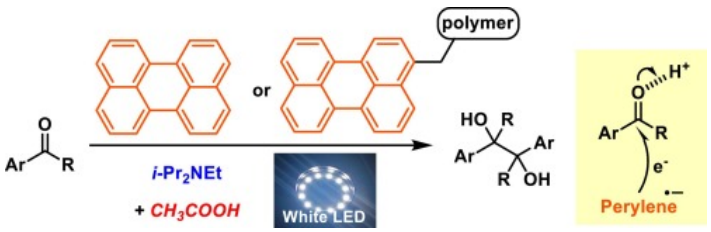

Abstract

A highly efficient and selective carbon–carbon double bonds cleavage of styrene compounds involving molecular oxygen was achieved using TBHP as a free radical initiator in diethylene glycol diethyl ether medium. Various styrene compounds, such as phenyl acrylic acids and its esters, 2-substituted 3-phenyl acrylic acids and its esters, chalcones, 4-phenyl-3-buten-2-one and bis(2-phenylvinyl) ketone, 5-benzylidene-1,3-dimethyl-pyrimidine-2,4,6-triones, could be effectively oxidized into the corresponding aryl carbonyl compounds, and the yield was up to 99%. A suitable mechanism was proposed. Gram-level synthesis further illustrated the practicality of our method.

Research article *Open access*

A simple method to obtain ursolic acid

Michael Azael Ludeña Huaman, Ana Luz Tupa Quispe, Reneé Isabel Huamán Quispe, Carlos Alberto Serrano Flores, Juana Robles Caycho

Article 100144

View PDF Article preview

Abstract

Abstract

A simple method has been developed to obtain ursolic acid (UA) by crystallization and recrystallization of the ethanol extract of *Clinopodium revolutum*. Its structure was confirmed by 1D (^{1}H-, ^{13}C-, DEPT 45, 90 and 135) and 2D (COSY, HMBC and HSQC) nuclear magnetic resonance (NMR) spectroscopy and Fourier transform infrared spectroscopy (FT-IR). The results provide a theoretical basis for considering the species *Clinopodium revolutum* with a source of UA.

Research article *Open access*

12-Phosphomolybdic acid $H_3[PMo_{12}O_{40}]$ over natural bentonite as a heterogeneous catalyst for the synthesis of 3,4-dihydropyrimidin-2-(1H)-ones

Lakha V. Chopda, Pragnesh N. Dave

Article 100169

View PDF Article preview

Abstract Graphical abstract

Graphical abstract

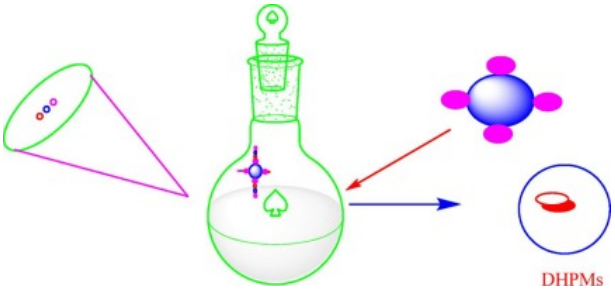

Research article *Open access*

Regioselective iodination of activated arenes using KI-DMSO in aqueous hydrochloride

Sainath Zangade, Pravinkumar Patil

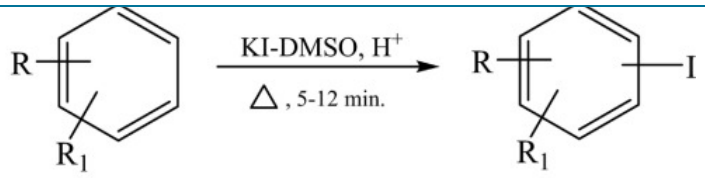

R = $COCH_3$, NH_2, OH, OCH_3, CHO
R_1= H, Cl, Br, OCH_3, NO_2.

Research article *Open access*

Synthesis, Spectral analysis and Anti-microbial properties of Cu, Ag, Au complexes of 2, 5-dihydroxy-1, 4-benzoquinone and 3, 6-dichloro-2, 6-dihydroxy-1, 4-benzoquinone

M. Amin Mir, Anuj Kumar, Shailendra P. Madwal, M.M.S. Jassal

Article 100209

View PDF Article preview

Abstract

Abstract

Many complexes of Cu, Ag, Au in combination with dianions derived from 2, 5-dihydroxy-1, 4-benzoquinone and 3, 6-dichloro-2, 6-dihydroxy-1, 4-benzoquinones have been synthesized and analysed for their antimicrobial activity. The I.R, ^{1}H and $^{13}CNMR$ data reveals that 2, 5-dihydroxy-1, 4-benzoquinone, coordinates as an O, O donor of the o-quinone type in *cis*-$Na_2[Cu_2O_5(HBQ)_2]$ $5H_2O$, cis-$(PPh_4)_2[Cu_2O_5(HBQ)_2]$, *cis*-$Na_2[Ag_2O_5(HBQ)_2]4H_2O$, *trans*-$AuO_2(HBQ).H_2O$ and chloranilate di-anion functions as an O, O ligand in *cis*-$Na_2[Cu_2O_5(DDB)_2]$ 6H2O, cis-$(PPh_4)_2[Cu_2O_5(DDB)_2]$ 4H2O, *cis*-$Na_2[AgO_2(DDB)_2]$, cis-$(PPh_4)_2[AgO_2(DDB)_2]$ $5H_2O$, trans-$(n\text{-}Bu_4N)_2[AuO_2(DDB)_2]3H_2O$. The complexes synthesized showed a good response as antimicrobial agents against the bacterial strains, viz, *Bacillus subtilis, Staphylococcus aureus, Xanthomonas malvacearum, E. coli,* Rhodococcus *sp, Pseudomonas putida.*

Research article *Open access*

Novel method for the synthesis of Sulfonamide Urea's from *p*-toluene sulfonyl isocyanate using Amberlite IRA-400 Cl resin: Application towards the synthesis of Gliclazide

Ravi Kumar Sadineni, Rajesh Kumar Rapolu, V.V.N.K.V. Prasada Raju, Srinivasu Navuluri, ... Naveen Mulakayala

Article 100217

View PDF Article preview

Abstract Graphical abstract

Graphical abstract

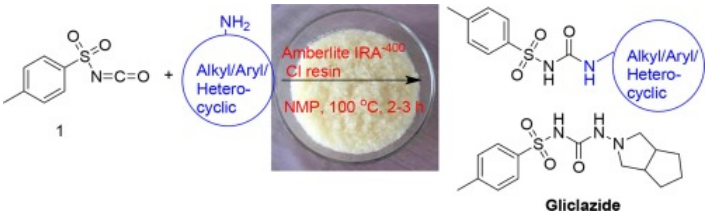

Research article *Open access*

A practical synthetic pathway of adamantylidene enol ethers by Wittig-Horner reaction has been developed. In this route, acetals were obtained by reaction of trimethyl orthoformate and benzaldehyde derivatives with tetrabutylammonium tribromide in methanol at room temperature. Trimethyl phosphite was converted into phosphonates with acetals in the presence of titanium (IV) tetrachloride in dichloromethane, followed by utilization of 2-adamantanone and lithium diisopropylamide (LDA) in anhydrous tetrahydrofuran under argon atmosphere at −78 °C to form adamantylidene enol ethers. Total yields are up to 66%.

Inorganic Chemistry

Research article *Open access*

Antioxidant, antibacterial and electrochemical activity of (E)-N-(4 (dimethylamino) benzylidene)-4H-1,2,4-triazol-4-amine ligand and its transition metal complexes

Md. Mahadi Hasan, Habib Md. Ahsan, Prianka Saha, Jannatul Naime, ... A.B.M. Nazmul Islam

Article 100115

View PDF Article preview

Abstract Graphical abstract

Graphical abstract

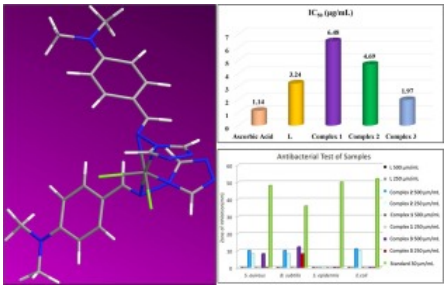

Research article *Open access*

2-Methoxy-5-(6-methoxypyridin-3-yl-imino-methyl)phenol and its transition metal complexes as potent antibacterial agents: Synthesis, characterization, theoretical investigations and biological evaluation

Vinusha Honnalagere Mariswamy, S. Bindya, Renyer A. Costa, Shashanka K Prasad, ... Shiva Prasad Kollur

Article 100120

View PDF Article preview

Abstract

Abstract

In this study, we have prepared an imine-based ligand, 2-methoxy-5-((6-methoxypyridin-3-ylimino)methyl)phenol (MIMP) and its Cu(II), Ni(II) and Zn(II) complexes in 2:1 stoichiometric ratio (2MIMP : Metal). The structure of obtained ligand and its metal complexes were elucidated with the aid of FT-IR, UV–Visible, NMR (^{1}H and ^{13}C) and mass spectra. Further, all the structures were analyzed via density functional theory (DFT) approach at B3LYP/LanL2DZ/6-311++G(2d,p) level, with HOMO-LUMO energies, geometric parameters, reactivity properties and electronic excitations obtained through TD-DFT calculations. Antibacterial activity of MIMP ligand and metal complexes have been evaluated via *in vitro* assays. In addition, the inhibition of the protein DNA gyrase-DNA complex was evaluated using molecular docking calculations, and the results revealed that biological accessibility of the metal complexes was better than ligand.

Abstract

This study investigated the effect of redox conditions on crystallization characteristics of anosovite in Ti-bearing titanomagnetite smelting slag. Under non-reducing conditions, besides anosovite, a part of Ti element was concentrated into rutile. Due to the much smaller particle size (within 10μm) of rutile than anosovite, anosovite was the better choice for selective liberation and separation, indicating that non-reducing conditions were not adequate. Under reducing condition, anosovite was the only Ti-rich phase and its liberation was excellent as the reduction degree ($n(Ti^{3+})/n(Ti^{4+}+Ti^{3+})$) was about 0.25. But when the reduction degree increased to 0.51, the liberation of the anosovite was poor because of the jagged grain boundary of anosovite particle. So from the liberation and separation perspective, reducing condition within a suitable degree was indispensable. In addition, as the redox conditions changed from oxidizing to reducing, the Ti level in the anosovite phase increased from 65.9% to more than 85%. Reducing condition is particularly favorable to increasing the content of TiO_2 in anosovite phase. Above all, a moderate reducing condition is a must for upgrading the Ti-bearing titanomagnetite smelting slag enough to be the worth resource.

Research article *Open access*

Relative reactivity of the dinuclear ruthenium complex $[CpRu(CO)_2]_2$ with diphenylselenyl sulphide and diphenyl disulphide

Wei Xiang Koh, Andrea Paris Gomez, Jiawen Lee, Jasmaadiyah Binte Habib Mohameed, Weng Kee Leong

Article 100159

View PDF Article preview

Abstract Graphical abstract

Graphical abstract

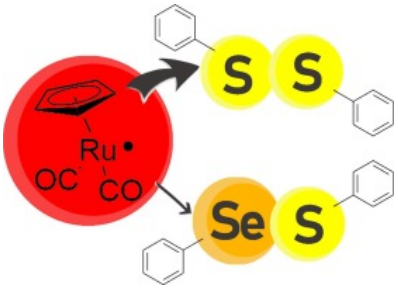

Research article *Open access*

Newly synthesized triazole-based Schiff base ligands and their Co(II) complexes as antimicrobial and anticancer agents: Chemical synthesis, structure and biological investigations

Sachin A. Deodware, Umesh B. Barache, Umakant B. Chanshetti, D.J. Sathe, ... Shiva Prasad Kollur

Article 100162

View PDF Article preview

Abstract

Abstract

The new Schiff base ligands 4-(2′/3′/4′-nitrobenzelideneimino)-3-methyl/ethyl-5-mercapto-1,2,4-triazole and their Co(II) metal complexes were synthesized and characterized by elemental analysis, magnetic moment measurements, thermal studies, electronic absorption and NMR spectroscopy. The ligands were synthesized by condensation of 4-amino-5-mercapto-3-methyl/ethyl-1,2,4-triazole with 2/3/4-nitrobenzaldehyde. On the basis of electronic absorption spectral data and magnetic susceptibility measurements, the octahedral geometry has been proposed for all the Co(II) complexes. Further, the ligands and Co(II) complexes have been screened for their antimicrobial activities against bacteria (*Staphylococcus aureus, Pseudomonas aeruginosa*) and fungi

Article 100188

View PDF Article preview

Abstract

Abstract

The convergence analysis of Ni (II) and Zn (II) and L- Glutamine complexes were studied using (0–50% v/v) dimethylformamide (DMF)-water mixtures potentiometrically at temperature 301.0K, having an ionic strength of 0.15 molL^{-1}. The complex species models were analysed by a well-defined computer Programme MINIQUAD75. Exhaustive modeling have been carried out on a number of complex species. The main complex species formed have been found of NiL_2, NiL_2H, NiL_2H_2, ZnL_2, ZnL_2H and ZnL_2H_2 type. On the basis of the statistical parameters the best fit chemical modelling have been applied. The statistical data analysis validated the complex species. The occurrence of columbic interactions over non-columbic interactions have been identified by linear variation stability of the medium with the help of mole fraction, and the preference of non-columbic interactions over columbic interactions as per linear variation of stability are because of dielectric constants of the medium.

Research article *Open access*

Characterization of chromium (III)-glycine complexes in an acidic medium by UV-visible spectrophotometry and capillary electrophoresis

Ariane Dasque, Marie Gressier, Pierre-Louis Taberna, Marie-Joëlle Menu

Article 100207

View PDF Article preview

Abstract

Abstract

Since the 2017 REACH restrictions on hexavalent chromium, the aeronautics industries have been seeking substitute processes for chromium plating. So far, use of trivalent chromium-based precursors seems to be the best solution in terms of process adaptation. The development of such processes requires a better understanding of plating bath solution chemistry. More specifically, there is a need to characterize the complexation mechanisms occurring with the chromium (III), since they are responsible for higher electrodeposition efficiency. Chromium (III) complexation occurs under specific conditions, such as in an acidic solution, where chromium hydrolysis takes place, leading to a stable aqua chromium complex, which is suspected to be detrimental to an even deposit. To tackle this issue, a complexing agent is added to destabilize hexaaquachromium complex. It is reported that ligands such as glycine allow the formation of chromium-ligand complexes under specific pH and chromium-ligand ratios. In order to identify and understand the formation of the various complexes, two characterization methods have been tested: UV–visible spectrophotometry, which allows identification of chromium complexes through d-d electronic transition in the UV–Visible range, and capillary electrophoresis as a separation method, coupled with UV–visible detection in order to

Research article *Open access*

Antimicrobial activities of Cu(II), In(III), and Sb(III) complexes of *N*-methyl-*N*–phenyl dithiocarbamate complexes

Timothy O. Ajiboye, Bukola O. Oluwarinde, Peter K. Montso, Collins N. Ateba, Damian C. Onwudiwe

Article 100241

View PDF Article preview

Abstract

Abstract

Dithiocarbamate compounds have interesting biological features, and have been considered as an alternative to conventional antibiotics in order to mitigate the spread of antimicrobial resistance. This accounts for the growing interest in the investigation

Analytical Chemistry

Research article *Open access*

A simple and economical ultrasound-assisted method for Cd and Pb extraction from fruits and vegetables for food safety assurance

Mónica Pereira, Florencia Tissot, Ricardo Faccio, Facundo Ibáñez, Mariela Pistón

Article 100089

View PDF Article preview

Abstract Graphical abstract

Graphical abstract

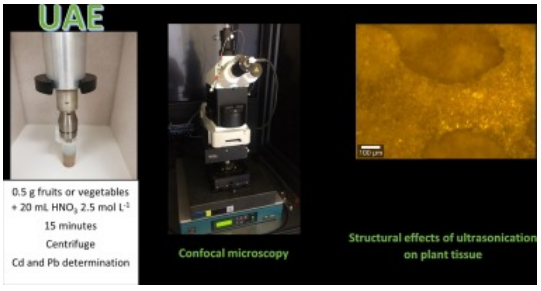

Research article *Open access*

Trace determination and speciation of elements in green tea

A. Hamza, S.O. Bahaffi, T.N. Abduljabbar, M.S. El-Shahawi

Article 100081

View PDF Article preview

Abstract

Abstract

The levels of some selected essential, non-essential, toxic elements and water-soluble inorganic anions (WSIAs) leached from green tea (GT) leaves infusion in boiled water at various time breaks were determined. A number of 29 GT samples were analyzed by Inductively Coupled Plasma-Mass/optical emission Spectrometry (ICP-OES/MS) and Ion chromatography (IC). The levels of studied elements and WSIAs (F^-, Cl^-, NO_3^-, PO_4^{3-} and SO_4^{2-}) leached from GT leaves in boiled water increased on growing infusion time. Chemical speciation (labile and complexed fractions) of P, Al, Cu, Pb and Cd in GT leaves in boiled water was estimated. At 95% confidence level ($P>0.50$), the student *t*-test values as calculated for essential and toxic metals were smaller than the critical value indicating no significant differences between element concentrations in the tested samples. The average daily dietary intake (ADDIs) for selected elements and the average daily intake (ADI) and the chronic reference dose (RFD) for Cd (μg kg^{-1} BW day^{-1}) were critically determined. Evaluation of inorganic composition allows quantification of the leaching percentage and the hazard beyond provisional acceptable average daily intake (ADI) values.

Research article *Open access*

Application of response surface methodology to optimize removal efficiency of water turbidity by low-cost natural coagulant (Odaracha soil) from Saketa District, Ethiopia

Yohanis Birhanu, Seyoum Leta

Article 100108

procedure for a jar test. 300 mL of water sample was added into a beaker by adjusting the water pH to the desired value. Different coagulant doses are added and mixed for 2 min by 250 rpm, then agitated for 10 min by 45 rpm. Finally, the sample was unflustered for different settling times. Response surface methodology (RSM) was also applied to optimize the process and estimate the interaction influence of the operating variables. According to the experimental result of this study, at the optimum condition (pH 7, 0.5 hrs settling time, and 3 g/L of coagulant dose), the turbidity removal efficiency of Odaracha was 88.13%. In contrast, the predicted turbidity removal efficiency was 90.54%, which indicates the consistency between the actual and the anticipated results. Correspondingly the R^2 value (0.9922) confirmed a high correlation between the real and predicted values. Generally, the quadratic model's actual and predicted results confirmed the turbidity removal capability of Odaracha and the

Research article *Open access*

Spectral analysis of total phosphorus in soils based on its diagnostic reflectance spectra

Pingping Fan, Xueying Li, Huimin Qiu, Guang-Li Hou

Article 100145

View PDF Article preview

Abstract

Abstract

Visible and near infrared spectroscopy (VNIR) has been successfully used to determine many soil parameters rapidly. However, total phosphorous (P) cannot be well quantified by VNIR, mainly because its absorption spectrum or reflectance spectrum was too weak to be studied. Here, we explored a new way to reveal the reflectance spectrum of total P in soils. Firstly, six types of soil residues were prepared after the original soil was sequentially extracted Ca_2-P, Ca_8-P, Al-P, Fe-P, O-P, and Ca_{10}-P, respectively. Secondly, the reflectance spectra of these P fractions were obtained using these soil residues by QE65000 spectrometer (Ocean Optics). Specifically, if we intended to get the spectrum of a certain P fraction, we would measure the reflectance spectrum of the soil residues without its neighboring former P fraction, using the soil residues after extracting this P fraction as the reference spectrum. Results showed that these P fractions had different characteristics of reflectance spectrum and can be well analyzed qualitatively and quantitatively. After summarizing the diagnostic spectra of these P fractions, the total P diagnostic spectrum was found to be distributed in 250–750 nm. Using these diagnostic bands, the spectral model of total P was established and showed a better result. This study provided an important evidence for understanding the characteristics of total P reflectance spectrum in

Research article *Open access*

Development and validation of LC-MS/MS method for quantification of ATP, ADP and AMP in dried blood spot, liver and brain of neonate mice pups

Richard L. Jayaraj, Hassib Narchi, Radhakrishnan Subramanian, Priya Yuvaraju

Article 100172

View PDF Article preview

Abstract Graphical abstract

Graphical abstract

View PDF Article preview

Abstract

Abstract

A new and sensitive (TLC) assay has been estimated for quantitation of synthetic binary mixtures of antipsychotic drug Amisulpride (AMS) with antimigarine drug Zolmitriptan (ZOL). These medications co-administered with each other for treatment of chronic migraine headache associated with psychosis. The synthetic mixture has been separated on precoated silica TLC plates G60 F254 by using mobile phase which consist of mixture of **Chloroform: Ethyl acetate: Methanol: Ammonia** in ratio (**30:30:73:3 v/v/v/v**). The mixture has been determined at λ_{max} 231 nm. Retardation factor (RF) values for AMS and ZOL have been 0.6 and 0.43 respectively. Calibration graphs have been linear in range 50–500 ng/spot for all studied drugs. The detection limits have been 6.04 & 10.5 ng/spot and the quantitation limits have been 18.3 & 31.834 ng/spot for AMS and ZOL respectively. The described assay has been utilized for quantitation of synthetic mixture in pharmaceutical tablet &biological fluids.

Research article *Open access*

Evaluating bioavailability of elements in municipal wastewater sludge (Biosolids) from three rural wastewater treatment plants in East Texas (USA) by a sequential extraction procedure

Kefa K. Onchoke, Oluwadamilola Olasumbo Fateru

Article 100211

View PDF Article preview

Abstract

Abstract

Biosolids (also known as sludge) are nutrient-rich materials used as soil amendments. A modified Tessier sequential extraction protocol was utilized for speciation and bioavailability of metals in samples from Nacogdoches and Lufkin wastewater sludges (NWWS, LWWS) and the Neches Compost sludge (NCS). Application of five steps (adsorbed, exchangeable, organically bound, carbonate and residual/sulfide) was performed to fractionate 26 elements (macroelements: Ca, Fe, K, Mg, Na, P, S, Li, Cs; microelements: As, B, Ba, Cd, Co, Cu, Hg, Mn, Mo, Pb, Se, V, Zn, Ni, Al, Cr, Sr) in samples via inductively coupled plasma optical emission spectrometry (ICPOES). The proximate amounts for most elements were predominant in the sulfide/residual fractions. Among macroelements 88.62–92.23% of K was found bioavailable vis-à-vis the organically-bound or sulfide fractions. About 100% of Li exists in the sulfide fractions vis-a-vis Group 2A elements. In contrast to microelements and transition metals, about 19–32 % Mo was found readily bioavailable. Additionally, Mo occurred in relatively lesser percent in sulfide/residual fractions vis-à-vis other elements. Cd, Pb, Co, V and Al were the least bioavailable. The percent relative bioavailabilities of microelements varied in the order:

Research article *Open access*

Development of a robust method for the determination of fluorine in liquid petroleum products

María Fernanda Gazulla, Marta Rodrigo, María Jesús Ventura, Cristina Andreu, Mónica Orduña

Article 100235

View PDF Article preview

Abstract

Abstract

A robust method for the determination of total fluorine in liquid petroleum products is developed. The methodology is based on the oxidative pyrohydrolytic combustion of the sample, followed by the analysis of the evolved gases absorbed in an absorbing solution by ion chromatography. The detection limit reached for fluorine is 0.5 $mg \cdot kg^{-1}$ and the quantification limit is 1.4 $mg \cdot kg^{-1}$, thanks to

Research article *Open access*

Separating the true from the false: A rapid HPTLC-ESI-MS method for the determination of cannabinoids in different oils

Theresa Schmidt, Jacqueline Stommel, Tim Kohlmann, Annemarie E. Kramell, René Csuk

Article 100234

View PDF Article preview

Abstract Graphical abstract

Graphical abstract

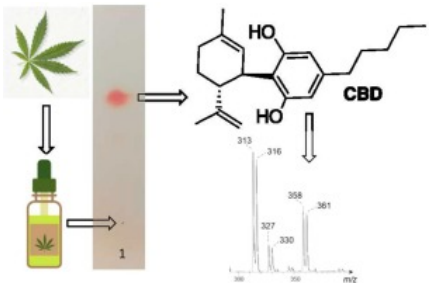

Electrochemistry

Research article *Open access*

N, O self-doped hierarchical porous carbon materials for high-performance super-capacitors

Liu Yang, Hong Zheng, Lian Liu, Wenjie Wu, Shuya Wang

Article 100109

View PDF Article preview

Abstract

Abstract

Biomass carbon materials have been widely used as electrode materials for super-capacitors (SC) due to their economic, environmental, and sustainable characteristics. In this work, we proposed that the Sapindus Mukorossi Peel (SMP) was used as a precursor to prepare a Sapindus Mukorossi Peel-based activated carbon material (SMPC) through carbonization and KOH activation. The morphology and structure of SMPC were characterized by various test methods. Cyclic voltammetry (CV), galvanostatic charge–discharge (GCD) and electrochemical impedance spectroscopy (EIS) were used to characterize its electrochemical performance. The results show that SMPC has suitable pore size distribution, a large number of heteroatom functional groups and excellent electrical conductivity. In addition, the amount of activator also has an important influence on the performance of SMPC. When the mass ratio of carbon material to KOH is 1:3, the prepared sample SMPC-3 has the largest specific surface area (SSA) was 1254.5 m^2/g. Moreover, SMPC-3 also has excellent electrochemical properties, high specific capacitance (at 1 A/g, the specific capacitance can reach 314.5F/g), good cycle stability (at 5 A/g, cyclic charge and discharge 5000 times, the specific capacitance is only lost by 4.2%.), superior rate performance (when the current density is increased from 0.5

Research article *Open access*

High-performance supercapacitor electrode materials of MoS_2/PPY nanocomposites prepared by *in-situ* oxidative polymerization method

Ling Li, Zhiqiang Wei, Jiahao Liang, Jinhuan Ma, Shangpan Huang

Article 100205

microscopy (HRTEM), X-ray photoelectron spectrometer (XPS). And the influence of the composite ratio on the electrochemical properties was evaluated by galvanizing charge–discharge (GCD), cyclic voltammetry (CV), electrochemical impedance spectra (EIS) and cycle stability. The experimental results show that all samples exhibit hexagonal systems with great crystallization. The morphologies are uniform structures with an obvious cladding layer. The CV curve is rectangular and the redox peak is evident. MoS_2 nanocomposites have excellent specific capacitance and good cyclic stability. The Nyquist spectrum of the sample shows that the electrical resistance of the MoS_2 nanocomposite is low and the electronic conductivity is excellent. When the current density is 1 A g-1, the specific capacitance of MP-2 is 677.8F g-1, which is higher than that of pure PPY and the other two kinds of nanocomposites. It can be seen from the experimental results that the specific capacitance of MP-2 nanocomposite material

Physical Chemistry and Chemical Physics

Research article *Open access*

Prediction of activities of all components in Sn-Ag-Cu and Sn-Ag-Cu-Zn lead-free solders using modified molecular interaction volume model

Yanjun You, Lingxin Kong, Junjie Xu, Baoqiang Xu, ... Bin Yang

Article 100143

View PDF Article preview

Abstract

Abstract

In this study, the activities of binary alloys (Sn-Ag, Sn-Cu, Sn-Zn, Ag-Cu, Ag-Zn, Cu-Zn) and ternary alloys (Sn-Ag-Cu, Sn-Ag-Zn, Sn-Cu-Zn) were predicted using molecular interaction volume model (MIVM), modified MIVM (M-MIVM), Wilson equation, and nonrandom two-liquid model. The prediction deviations of the M-MIVM were the smallest among the four thermodynamic models, indicating that the M-MIVM is reliable for predicting the activity of these multicomponent lead-free solders. On this premise, the activities of all components in ternary Sn-Ag-Cu solders at 1300 K were predicted using the M-MIVM. We found that the activities of Sn, Ag and Cu exhibit negative deviations from Raoult's law and that these deviations eventually transform into positive deviations. The activities of all components in quaternary Sn-Ag-Cu-Zn solders at 1000 K were also predicted using the M-MIVM when Zn contents were 0.1 and 0.2. This study provides a complete thermodynamic description of Sn-Ag-Cu ternary and Sn-Ag-Cu-Zn quaternary alloys.

Research article *Open access*

Photophysical and molecular docking studies of photoinduced electron transfer (PET) and non-PET based fluorophores of acridinedione derivatives with a glycoprotein: Ovalbumin

Anupurath Sumita, Gunasekaran Shoba, Ramachandran Thamarai Selvan, Krishnan Anju, ... Rajendran Kumaran

Article 100187

View PDF Article preview

Abstract

Abstract

Photophysical studies of resorcinol-based family of acridinedione (ADR) dyes with a glycoprotein, ovalbumin (OVA) were carried out in water. Addition of OVA to photoinduced electron transfer (PET) based dye (ADR1) resulted in a considerable red shift of emission maxima with a slight increase in the fluorescence intensity, whereas no significant variation in the fluorescence intensity or shift of emission maxima results in the case of a non-PET dye. Fluorescence lifetime studies illustrates that the PET lifetime component enhances by several fold on the introduction of OVA which is accompanied with the formation of multi lifetime components in the aqueous phase of varying distribution as observed in well-known globular protein, bovine serum albumin (BSA). Interestingly, a decrease in the fluorescence lifetime of non-PET dye (ADR2) with the evolution of more than one distinct lifetime species results with OVA. This behaviour ascertains the presence of at least two different micro environment of

David Arturo Munar-Florez, Darlis Adriana Varón-Cardenas, Nidia Elizabeth Ramírez-Contreras, Jesús Alberto García-Núñez

Article 100119

View PDF Article preview

Abstract

Abstract

This study investigated the effects of production conditions on the ammonium and phosphate adsorption capacity of oil-palm-shell-biochar. Biochar was prepared at three pyrolysis temperatures (350, 650, and 750 °C), under three activation conditions (no oxidation, partial oxidation at 250 °C, and chemical activation with K_2CO_3), and using three washing methods (no washing, acid washing, and hot water). Physicochemical properties of certain biochar samples were characterized by SEM, CHON-S, XRF, FTIR, and area BET. The highest ammonium adsorption capacity (1.49 mg/g) was observed for chemically activated biochar pyrolyzed at 650 °C without washing. The best phosphate adsorption capacity (0.89 mg/g) was observed for partially oxidized biochar pyrolyzed at 650 °C with acid washing. The BET surface area ranged from 4 to 253 m^2/g. The biochar produced at 350 °C without washing had more surface functional groups than that produced at higher temperatures. The chemical activation process promoted the development of numerous functional groups on the biochar surface.

Research article *Open access*

MHD heat and mass transport of Maxwell Arrhenius kinetic nanofluid flow over stretching surface with nonlinear variable properties

S.O. Salawu, E.O. Fatunmbi, S.S. Okoya

Article 100125

View PDF Article preview

Abstract

Abstract

The study of nonlinear radiation and mixed convection of the MHD heat and mass transfer of Maxwell nanoliquid flow in porous media with Arrhenius kinetic reaction is examined. The non-Newtonian fluid is characterized by Maxwell model, and the species molecular mixture is inspired by the Arrhenius pre-exponential kinetics. Reaction mixture occurs in a boundless slippery plate subject to a considerable quantity of tension that can prevent material deformity. With appropriate similarity variables, the flow model reduces to quasilinear coupled system of derivatives. A numerical simulation of the flow characteristics is carried out, and the results presented in tables and graphs for various thermodynamic phenomena. The results show that the flow momentum is damped by the material term, but augmented by nonlinear heat convection and radiation. The heat transfer rate is significantly propelled by temperature ratio and viscous heating, while the Lewis number, molecular Brownian motion and the chemical reaction term encourage species mass transfer. As such, the study involving activation energy plays a critical part in the diffusion of binary chemical mixtures of energy and species transport which will assist the chemical engineering and others in their activities to prevent reaction blowup.

Research article *Open access*

Characterization and biological activities of synthesized citrus pectin-MgO nanocomposite

R. Supreetha, S. Bindya, P. Deepika, H.M. Vinusha, B.P. Hema

Article 100156

View PDF Article preview

Abstract

Abstract

biological activity data showed that the citrus pectin-MgO nanocomposite is more potent than the pectin.

Research article *Open access*

Synthesis of a Divinyl-functionalized Diamantane-Analogue from naturally occurring *myo*-Inositol and its application to polymer synthesis via the Thiol-ene reaction

Kimikatsu Ikeya, Shusuke Okamoto, Atsushi Sudo

Article 100167

View PDF Article preview

Abstract Graphical abstract

Graphical abstract

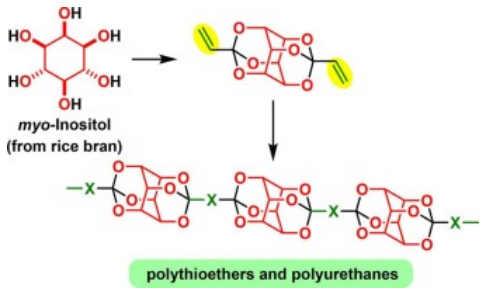

Theoretical and Computational Chemistry

Research article *Open access*

FT-IR, FT-Raman, UV–Visible, NMR, DFT and molecular docking investigation of 1-(phenyl (piperidin-1-yl) methyl) naphthalene-2-ol

P. Rajamani, V. Vijayakumar, N. Sundaraganesan, Mani Jeeva, Maria Susai Boobalan

Article 100096

View PDF Article preview

Abstract

Abstract

1-(Phenyl(piperidin-1-yl)methyl)naphthalene-2-ol was synthesized and characterized utilizing spectroscopic techniques (FT-IR, FT-Raman, UV–Visible, NMR, Mass and CHNS analysis). The synthesized compound chemical structure was optimized using the Density Functional Theory (DFT) B3LYP/6-311G (d,p) basis set. The computational studies including NMR chemical shift value, vibrational frequencies, natural bond orbital (NBO), frontier molecular orbital (FMO), molecular electrostatic potential (MEP), HOMO-LUMO, NLO, dipole moment, Mulliken charge analysis, thermal studies and potential energy surface (PES) analysis. Molecular docking studies were also carried out for Haemophilus influenza protein with target molecule using Autodock 4.2 versions and showed potential inhibitor activity against Haemophilus influenzae diseases.

Research article *Open access*

^{13}C NMR chemical shift assignments of nitrated benzo[a]pyrenes based on two-dimensional techniques and DFT/GIAO calculations

Kefa K. Onchoke

Article 100099

spectroscopy (HMQC and HMBC) were carried out. Further, the computation of fifty ^{13}C chemical shifts of 1-, 3-, and 6-nitrobenzo[a]pyrenes by using GIAO B3LYP/6-311+G(d,p)//B3LYP/6-31+G(d), 6-31+G(d,p), 6-311+G(d), 6-311+G(d,p), 6-311G(d,p) levels of theory was investigated. For 1-, 3- and 6-NBaP the calculated chemical shifts δ_{calc} versus δ_{expt} plots of chemical shifts fall on a linear correlation line with $r^2>0.90$. The GIAO B3LYP/6-311+G(d,p)//B3LYP/6-311G(d,p)level of theory was found to yield chemical shifts in good agreement with experiment with $r^2>0.90$. The most expensive method (larger basis set) has provided the best agreement with the experiment. It is therefore important to continue to seek computational methods that can predict precise chemical shifts in nitrated or related compounds.

Research article *Open access*

Computational prediction of hERG blockers using homology modelling, molecular docking and QuaSAR studies

Nataraj Sekhar Pagadala

Article 100101

View PDF Article preview

Abstract

Abstract

A full-length three-dimensional structure of the tetrameric potassium ion channel (hERG Kv11.1) including the N- and C-terminal domains was built, with a diameter of 6Å and 12Å between the K+selectivity filter and the pore cavity residue Tyr^{652} of opposite subunits. Further docking studies with a set of 233 structurally known blockers have shown that compounds bind near the inner vestibule of the pore channel, as well as the helix-IV region of the voltage sensor domain (VSD) in the alpha subunit. The residues of hERG, Gly^{626}, Phe^{627}, Gly^{628}, Tyr^{652} and Phe^{656} of the pore channel and Arg^{488} of VSD plays an important role in ligand binding and hERG blockage. The conducted QuaSAR model is statistically significant, with R^2 of 0.72 in predicting the hERG blocking activity. Furthermore, QuaSAR descriptors employing computer-assisted multiple regression procedure reveal that increase in hydrophobicity with higher number of aromatic rings are favorable for the binding affinity of hERG blockers. Additionally, the pIC_{50} values of 25 commercial compounds screened using structure-based pharmacophore model also show binding to the selectivity filter and pore cavity of hERG potassium channel like the known hERG blockers with a wide range of inhibition from weak to strong blockage predicting to have proarrhythmic potential.

Catalysis

Research article *Open access*

Selective oxidation of benzyl alcohols with molecular oxygen as the oxidant using Ag-Cu catalysts supported on polyoxometalates

Simon Lukato, Ola F. Wendt, Reine Wallenberg, Gabriel N. Kasozi, ... Emmanuel Tebandeke

Article 100150

View PDF Article preview

Abstract

Abstract

We report an efficient process for the oxidation of benzyl alcohols using molecular oxygen as the oxidant catalyzed by Ag-Cu catalysts supported on polyoxometalates (Ag-Cu/POM). The Ag-Cu/POM catalyst was prepared by galvanic displacement in the presence of polyvinyl pyrrolidone and polyethylene glycol. The catalysts were characterized using Fourier transform infrared spectroscopy (FTIR), ultraviolet–visible spectroscopy (UV–Vis), powder X-ray diffraction (PXRD), X-ray fluorescence (XRF), Brunauer-Emmett-Teller (BET) surface analysis, transmission electron microscopy (TEM), energy dispersive spectroscopy (EDS) and thermogravimetric analysis (TGA). The oxidation reaction was carried out using a Schlenk– line setup, under ambient atmospheric pressure. Reaction products were identified by GC–MS and quantified with GC using an internal standard method. The Ag-Cu/POM catalyst gave close to 100% benzyl alcohol conversion in 5h with >99% selectivity to benzaldehyde. When tested on various benzyl alcohol derivatives the Ag-Cu catalysts showed good conversions and >99% selectivity to the corresponding

Abstract Graphical abstract

Graphical abstract

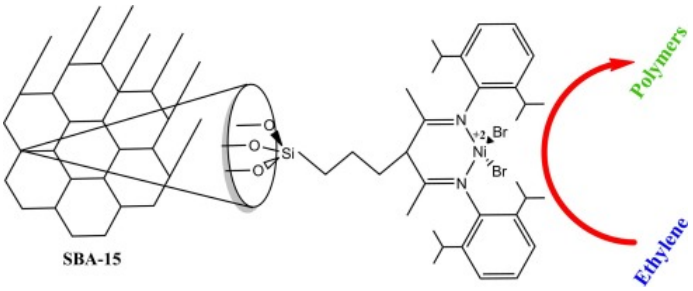

Green and Sustainable Chemistry

Research article *Open access*

Sulfated TiO_2/SnO_2 nanocomposite as a green heterogeneous catalyst for direct amide formation reaction

S.M. Patil, S.A. Vanalakar, S.A. Sankpal, S.P. Deshmukh, S.D. Delekar

Article 100102

View PDF Article preview

Abstract

Abstract

Heterogeneous binary TiO_2/SnO_2 nanocomposite (with 4:1 wt% of TiO_2 and SnO_2, respectively) catalyst was prepared by a sol–gel method, and further sulfated by chlorosulfonic acid. X-ray diffraction technique revealed the structure of the nanocrystalline catalyst to be tetragonal. Fourier transformed infrared technique elucidated the presence of surface-anchored sulfonic ($-SO_3H$) groups on the catalyst. Morphological details of the catalyst were obtained by transmission electron microscopy. Elemental analysis of the catalyst was carried out by X-ray photoelectron spectroscopy. NH_3-TPD technique was used to elucidate the surface acidity of the catalyst. The active surface area and mesoporosity of catalyst were studied by the BET method. Thereafter, this sulfated catalyst was utilized for the direct amidation reaction between a series of amine derivatives and acetic acid. The reaction gives excellent product yield within 120 min, and at a relatively moderate temperature of ~115 °C.

Research article *Open access*

Purification of xylooligosaccharides from bamboo with non-organic solvent to prepare food grade functional sugars

Yetao Jiang, Xiaoyu Wang, Zhen Wu, Jiaxing Xu, ... Lu Lin

Article 100153

View PDF Article preview

Abstract

Abstract

Food grade xylooligosaccharides (XOS) have a high application value, but most of the reported purification methods of XOS use organic solvents, which has significant problems such as large amount of solvent, residual solvent, and difficulty in solvent recovery. In addition, although there are many reported methods of separation and purification, quantitative analysis is lacking for each specific treatment step, such as sugar loss rate, decolorization rate, protein removal rate, and desalination rate. Therefore,

Proficient synthesis of zinc oxide nanoparticles from *Tabernaemontana heyneana* Wall. via green combustion method: Antioxidant, anti-inflammatory, antidiabetic, anticancer and photocatalytic activities

D.J. Manasa, K.R. Chandrashekar, M.A. Pavan Kumar, D. Suresh, ... H.C. Ananda Murthy

Article 100178

View PDF Article preview

Abstract

Abstract

The zinc oxide nanoparticles (*T*-ZnO NPs) were synthesized successfully by the application of leaf, stem and callus extracts of *Tabernaemontana heyneana* Wall. via the green combustion method. The structural, bonding and morphological features of *T. heyneana* mediated ZnO NPs (*T*-ZnO NPs) were explored using XRD (X-ray powder diffraction), UV–Vis (Ultra-violet visible spectroscopy), FESEM-EDS (Field Emission-SEM and energy-dispersive X-ray spectra), DLS (Dynamic light scattering) and FTIR (Fourier transform infrared) techniques. UV–Vis spectra revealed the presence of a band in the region between 370 and 376 nm approving the presence of *T*-ZnO NPs. XRD, FESEM-EDS, TEM and DLS analysis confirmed the formation of nanosized, spherical shaped, highly stable and pure crystalline wurtzite *T*-ZnO NPs. FTIR spectra revealed the presence of most probable phytochemicals from plant extracts involved in the processes of reduction and stabilization of *T*-ZnO NPs. The *T*-ZnO NPs could effectively inhibit the activity of DPPH (1, 1-Diphenyl-2-picrylhydrazyl) radical (IC_{50} value between 467.7 and 752.3 µg/ml) exhibiting potent radical scavenging activity. The *T*-ZnO NPs exhibited strong anti-inflammatory (membrane stabilization) activity. The antidiabetic potential of *T*-ZnO NPs was assessed and found to exhibit excellent α-glucosidase (IC_{50} at 16.3 µg/ml)

Research article *Open access*

Natural surfactants assisted an efficient synthesis of tetrahydro-β-carbolines

Somnath S. Gholap, Vinod R. Kadu

Article 100183

View PDF Article preview

Abstract

Abstract

An expeditious protocol for the synthesis of structurally diversified β-carboline derivatives has been reported using a readily available natural surfactant medium. The synthesis of β-carboline derivatives in good yields under optimized conditions was carried out by the reaction of tryptamine with aldehydes in an aqueous extract of *Acacia Concinna* pods. The use of an aqueous medium, ease of purification, good yield and cost-effective reaction suggest for bulk scale production β-carboline derivatives.

Supramolecular Chemistry

Research article *Open access*

Enhanced multifunctionality of CuO nanoparticles synthesized using aqueous leaf extract of *Vernonia amygdalina* plant

H.C. Ananda Murthy, Tegene Desalegn Zeleke, K.B. Tan, Suresh Ghotekar, ... C.R. Ravikumar

Article 100141

View PDF Article preview

Abstract

Abstract

We report the synthesis of medicinal plant, *Vernonia amygdalina Del.* mediated green copper oxide nanoparticles (*VeA*-CuO NPs). The presence of two absorbance maxima, λmax 1 and λmax 2 at 436 nm and 452 nm, respectively confirms a mixture of

Medicinal Chemistry and Chemical Biology

Research article *Open access*

In-silico drug repurposing study: Amprenavir, enalaprilat, and plerixafor, potential drugs for destabilizing the SARS-CoV-2 S-protein-angiotensin-converting enzyme 2 complex

Ivonne Buitrón-González, Giovanny Aguilera-Durán, Antonio Romo-Mancillas

Article 100094

View PDF Article preview

Abstract Graphical abstract

Graphical abstract

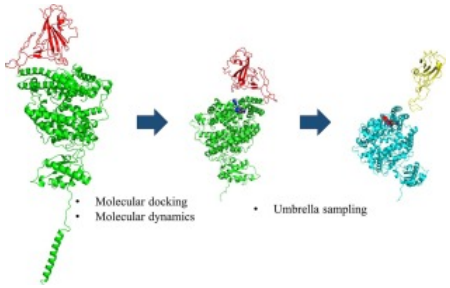

Research article *Open access*

Click chemistry: In vitro evaluation of glycosyl hybrid phosphorylated/thiophosphorylated 1,2,3-triazole derivatives as irreversible acetyl cholinesterase (AChE) inhibitors

B. Anjaneyulu, G.B. Dharma Rao, Tanima Bajaj

Article 100093

View PDF Article preview

Abstract

Abstract

A novel series of phosphorylated/ thiophosphorylated glucosyl-1,2,3-triazole derivatives have been synthesized in three step process. The synthetic approach was progressed from the reaction of propargyl alcohol with dialkoxychlorophosphate/thiophosphate derivatives to give propargylphosphate/thiophosphate derivatives. Then, the reaction of above synthesized compounds with acetylated glucosyl azides through azide-alkyne [2+3]-cycloaddition reaction (click reaction) led to the formation of the title phosphorylated/thiophosphorylated glucosyl-1,2,3-triazole derivatives in good yields. The synthesized compounds are subjected to biological evaluation as acetyl cholinesterase (AChE) inhibitors and the results are compared with reported compounds.

Research article *Open access*

Synthesis, characterization of novel Sesamol substituted with thiazolidin-4-one derivatives and their evaluation for anti-oxidant and anti-cancer activities

N.L. Yaswanatha Kumar,, Kumar K.N. Bharathi, Jayesh Mudgal, S.G. VasanthaRaju, S.A. Manohara Reddy

Article 100095

Research article *Open access*

Evaluation of the antioxidant activities of aqueous extracts from seven wild plants from the Andes using an *in vivo* yeast assay

Miki Gonzales, Gretty K. Villena, Ana A. Kitazono

Article 100098

View PDF Article preview

Abstract

Abstract

The antioxidant activities of the aqueous extracts of seven wild plants were investigated, using both *in vitro* and *in vivo* assays. The former relied on the use of 2,2-diphenyl-1-picrylhydrazyl (DPPH) and the latter, on the sensibility towards hydrogen peroxide of the yeast *sod1* mutant. The studied plants were all wild, collected at the Ccamarrara hill (4000 m.a.s.l. Cusco, Peru), and of the following species: *Plantago australis*, *Baccharis latifolia*, *Ageratina sternbergiana*, *Stevia macbridei*, *Ageratina cuzcoensis*, *Calceolaria myriophylla,* and *Adiantum orbignyanum*. The DPPH assay demonstrated high antioxidant contents in the dry leaves of all tested plants, with AAEAC values (ascorbic acid equivalent antioxidant capacity) ranging from 20.6 to 72.7 mg/g dry leaves. The antioxidant activities were also evident in the yeast assay, which also allowed distinction between the intracellular and extracellular effects. These *in vitro* and *in vivo* studies demonstrate the need to further investigate native wild plants from the Andes as important sources for water-soluble antioxidant compounds.

Research article *Open access*

Anticancer potential of 3-hydroxypyridine-2-carboxaldehyde N(4)-methyl and pyrrolidinylthiosemicarbazones and their Zn(II) complexes in different cancers via targeting MAPK superfamily signaling pathway

Nerina Shahi, Vivek Pandey, Ankita Pathak, Ram Sundar Thapa, ... Paras Nath Yadav

Article 100104

View PDF Article preview

Abstract Graphical abstract

Graphical abstract

Schematic representation of mechanism of action of HHyPyPyrd on cancer cell proliferation.

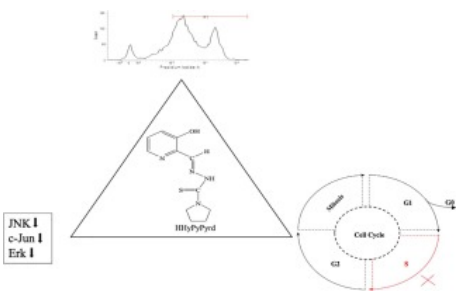

Abstract

Investigation of ultraweak photon emission (UPE) in living mater was started in 1920-s by Russian biologist A. Gurwitsch discovered mitogenetic radiation (MGR), ultraviolet light emitted from growing organisms that stimulated similar organisms to grow. MGR attracted enormous interest of the scientific community resulting in many scientific publications confirming occurrence of permanent and spontaneous biophoton emission during natural metabolic processes in diverse living organisms. However, along with studies showing the existence of intercellular electromagnetic communication resulted in various responses of detector cells there have been numerous unsuccessful attempts to confirm the biological significance of MGR. Here we reported strong evidence for non-chemical intercellular signaling leading to biological cellular response. We found the ability of various cell types under conditions of oxidative stress induced by p-benzoquinones to generate death signals, which can affect target cells over long distances through non-aquatic environments resulting in morphological alterations and viability loss. We show that detector cells may distinguish and respond the same way to death signals transmitted from various type of inducer cells and pharmaceuticals may interrupt cellular death responses. These findings provide strong support for the view that non-

Research article *Open access*

An integrated virtual screening of compounds from *Carica papaya* leaves against multiple protein targets of SARS-Coronavirus-2

Pandu Hariyono, Christine Patramurti, Damiana S. Candrasari, Maywan Hariono

Article 100113

View PDF Article preview

Abstract

Abstract

The pandemic of SARS-Coronavirus-2 (Coronavirus-19) has been progressing by the increasing trend of the cases as well as deaths with neither vaccine nor drug is rationally used to stop the viral spread over. This study aims to perform an integrated virtual screening of compounds that had been identified from *Carica papaya* leaves, which are proposed to be a herbal treatment for SARS-Coronavirus-2. The screening was initiated by evaluating the 40 compounds from *Carica papaya* leaves for their drug-like likeness property. The selected compounds were then secondly screened using carcinogenic and toxicity filters. Further selected compounds were thirdly screened for their pharmacokinetic profile and the screening was lastly performed by docking the third selected compounds against multiple protein targets of SARS-Coronavirus-2 employing 3-chymotrypsin-like protease (3CLpro), papain-like protease (PLpro), RNA-dependent-RNA-polymerase (RdRp), endonuclease (EndoU), S1 and S2 region of spike protein. The results show that 20 of 40 compounds, which meet the requirements of drug-like likeness, carcinogenicity-toxicity filter, and pharmacokinetic profiles, can interact with the multiple protein targets of SARS-Coronavirus-2 with the order from high to low affinity as follows: S1>3CLpro>EndoU>RdRp>PLpro>S2. In conclusion, *Carica papaya* leaves are worth to be proposed for

Research article *Open access*

Design and synthesis of novel estrogen receptor antagonists with acetal containing biphenylmethane skeleton

Materu Yuyama, Takashi Misawa, Yosuke Demizu, Takayuki Kanaya, Masaaki Kurihara

Article 100124

View PDF Article preview

Abstract Graphical abstract

Graphical abstract

Biosynthesis and characterization of nickel oxide nanoparticles by using aqueous grape extract and evaluation of their biological applications

Baraa Y. Hussein, Ahmed Mishaal Mohammed

Article 100142

View PDF Article preview

Abstract Graphical abstract

Graphical abstract

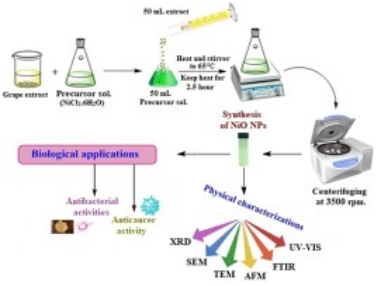

Research article *Open access*

Synthesis, anticancer and larvicidal activities of a novel Schiff base ligand, 3-((2-((1-(4-hydroxyphenyl)ethylidene)amino)ethyl)imino)-N-(p-tolyl)butanamide and its Mn(II), Fe(III), Co(II), Ni(II) and Zn(II) complexes

K. Subin Kumar, V.N. Reena, K.K. Aravindakshan

Article 100166

View PDF Article preview

Abstract

Abstract

A novel Schiff base ligand, *3-((2-((1-(4-hydroxyphenyl)ethylidene)amino)ethyl)imino)-N-(p-tolyl)butanamide* (**H_2L**) and its some metal, Mn(II), Fe(III), Co(II), Ni(II) and Zn(II) complexes have been synthesized. Schiff base ligand was characterized by analytically and HRMS, IR-, ^{1}H NMR, ^{13}C NMR- and UV–Vis spectral techniques. In addition to this molar conductance and magnetic moment calculations were used to characterize metal complexes. The ligand and its complexes have been evaluated for their *in vitro* cytotoxicity against Dalton's Lymphoma Ascites (DLA) cell lines by Trypan Blue Exclusion method. Zn(II) complex was selected to evaluate its efficiency against EAC (Earlich Ascites Carcinoma) induced ascites tumor and DLA induced solid tumor in Swiss Albino female mice. The results are expressed with an IC_{50} value, 48µg/ml, which indicated that Zn(II) complex showed as a potential anticancer agent. Metal complexes of Mn(II), Fe(III), Co(II), Ni(II) and Zn(II) are taken to examine for their larvicidal activity against larvae of *Cx. quinquefasciatus*. The statistically analyzed results showed that the sample of Zn(II) complex exhibited potential larvicidal activity.

Research article *Open access*

Use of molecular homology model to identify inhibitors of *Staphylococcus pseudintermedius* sortase A

Manasi Balachandran, Jerome Baudry, Stephen A. Kania

Article 100185

View PDF Article preview

Abstract

level of transcription determined in isolates representing major clonal complexes. The gene was synthesized and then expressed in *Escherichia coli* and the recombinant enzyme's activity measured using a synthetic substrate. A three dimensional homology model of SrtA was generated and used in virtual screening libraries of chemicals for potential inhibitors. Four compounds that showed 50% or greater inhibition of SrtA activity were identified. A thermal shift assay confirmed binding of one inhibitor to the

Research article *Open access*

Potential SARS-CoV-2 3CLpro inhibitors from chromene, flavonoid and hydroxamic acid compound based on FRET assay, docking and pharmacophore studies

Maywan Hariono, Pandu Hariyono, Rini Dwiastuti, Wahyuning Setyani, ... Habibah Wahab

Article 100195

View PDF Article preview

Abstract

Abstract

This present study reports some natural products and one hydroxamic acid synthetic compound which were previously reported as matrix metalloproteinase-9 (MMP-9) inhibitors to be evaluated for their inhibition toward severe acute respiratory syndrome coronavirus-2 (SARS-CoV-2) 3-chymotrypsin-like protease (3CLpro). This enzyme is one of the proteins responsible for this coronaviral replication. Two herbal methanolic extracts i.e., *Averrhoa carambola* leaves and *Ageratum conyzoides* aerial part demonstrate >50% inhibition at 1000μg/mL. Interestingly, apigenin, one of flavonoids, demonstrates 92% inhibition at 250μg/mL (925μM) as well as hydroxamic acid compound, *N*-isobutyl-*N*-(4-methoxyphenylsulfonyl)glycyl hydroxamic acid (NNGH), which shows 69% inhibition at 100μM. The *in vitro* results are supported by the docking studies revealing that the binding mode of both compounds is mainly by interacting with GLU166 residue in the hydrophobic pocket of the 3CLpro. Pharmacophore mapping further supported the results by confirming that the *in vitro* activities of both compounds are due to their pharmacophore features employing hydrogen bond acceptor (HBA), hydrogen bond donor (HBD) and hydrophobic. Gas Chromatography-Mass Spectrometry (GC–MS) analysis reported chromene compounds in *Ageratum conyzoides* aerial part methanolic extract are

Research article *Open access*

A *N*-(4-chlorophenyl)-γ-amino acid derivatives exerts *in vitro* anticancer activity on non-small cell lung carcinoma cells and enhances citosine arabinoside (AraC)-induced cell death via mitochondria-targeted pathway

Povilas Kavaliauskas, Šarūnas Žukauskas, Kazimieras Anusevičius, Benas Balandis, ... Vytautas Mickevičius

Article 100193

View PDF Article preview

Abstract Graphical abstract

Graphical abstract

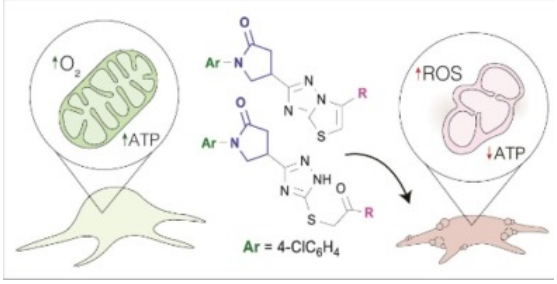

Abstract

The constant emergence of drug-resistant strains of bacteria places a sustained burden on mankind as most antibiotics commonly used for treating bacterial infections are no longer efficient. This poses an urgent need for a new and effective class of antibacterial agents. Nitrogen-containing heterocycles have been found to have the most comprehensive spectrum of biological activities. Herein, we propose the route to access pyrazinoindole derivatives and evaluated them for *in-vitro* antibacterial activity. Synthesized analogs were tested for their antimicrobial activity against two gram-negative and two gram-positive bacteria. The range of minimum inhibitory concentration (MIC) was found in between 3.75 and 60μg/mL where gentamycin was used as a standard drug. The structure-activity relationship studies also depicted the correlation of the electronic parameters with the antibacterial activity of the target compounds. Our findings were further confirmed using *in-silico* assays and favourable results were obtained in accordance with experimental outcomes. We mechanistically revealed that pyrazinoindole based compound **4g** has strong non-covalent interactions by using H-bonds and hydrophobic interactions through molecular dynamics simulation studies, making it potential antibacterial compound. Further, results were strengthen by energy landscape which showed the

Micro article

Others

Research article *Open access*

Solvent-free one pot synthesis of 1,2-dihydroquinolines from anilines and acetone catalysed by MOF-199

Vrushali Raut, Rucha R. Wani, Hemchandra K. Chaudhari, Dipanwita Das

Article 100097

View PDF Article preview

Abstract Graphical abstract

Graphical abstract

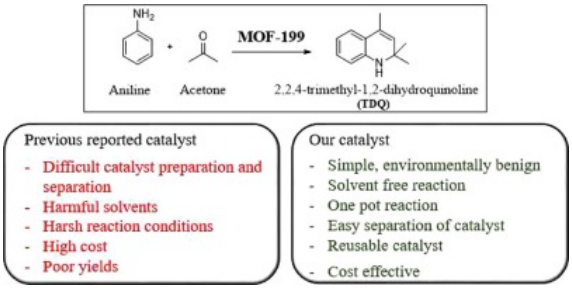

Research article *Open access*

Synthesis, characterization, anti-inflammatory evaluation, molecular docking and density functional theory studies of metal based drug candidate molecules of tenoxicam

Harun Muslu, Zeynep Kalaycıoğlu, Taner Erdoğan, Ayşegül Gölcü, F. Bedia Erim

Article 100111

View PDF Article preview

Abstract Graphical abstract

Graphical abstract

Synchrotron-based X-ray microscopy for assessing elements distribution and speciation in mangrove tree-rings

Elton Eduardo Novais Alves, Daigard Ricardo Ortega Rodriguez, Pablo de Azevedo Rocha, Leonardus Vergütz, ... Liovando Marciano da Costa

Article 100121

View PDF Article preview

Abstract Graphical abstract

Graphical abstract

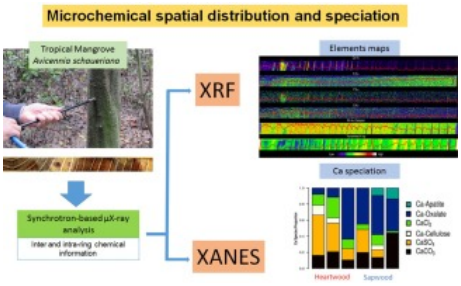

Research article *Open access*

HPLC-PDA combined with chemometrics for chemical markers of Paeoniae Radix Alba before and after sulfur-fumigated

Xiaozhou Jia, Yueyi Liang, Fang Chen, Xiaoxia Liu, ... Mei Wei

Article 100155

View PDF Article preview

Abstract

Abstract

To quantitatively compare the chemical composition of Paeoniae Radix Alba before and after sulfur-fumigated by using HPLC fingerprint and chemometrics, to provide a reference for the quality evaluation of Paeoniae Radix Alba. Establish the fingerprints of 9 batches of white peony and its sulfur-fumigated products, combined with orthogonal partial least squares-discriminant analysis (PLS-DA) to compare the composition differences of white peony before and after sulfur-fumigation. For the quantitative analysis of sexual components, differential compounds were identified by UPLC-MS. The contents of gallic acid, catechins, albiflorin, paeoniflorin, 1,2,3,4,6-pentagalloyl glucose and benzoylpaeoniflorin before and after sulfur-fumigation Paeoniae Radix Alba were determined, and there were 6 common peaks in the HPLC fingerprints of Paeoniae Radix Alba before and after sulfur-fumigated. There were 6 common peaks in Paeoniae Radix Alba without sulfur-fumigated, and 7 peaks after sulfur-fumigated. The differential compound (peak 7) was proven to be paeoniflorin sulfite.The differential compound was proven to be paeoniflorin sulfite. This method can be used for fingerprint analysis and quantitative analysis of different components of Paeoniae Radix Alba and sulfur-fumigated Paeoniae Radix Alba, and can distinguish Paeoniae Radix Alba from sulfur-fumigated

Organic Chemistry

Open access

Synthesis, spectral characterizations and biological applications of novel 3-[(*E*)-(4, 6-dihydroxy pyrimidin-5-yl)diazenyl]-4-methylbenzoic acid azo Dye and their derivatives

A.G. Prashantha, J. Keshavayya, R.A. Shoukat Ali

Article 100110

aminopyrimidine-4,6-diol(**4**) under suitable experimental condition. The azo dyes obtained are orange-red in color and they are characterized by various analytical methods like IR, UV–Vis, ^{1}H NMR, ^{13}C NMR and Mass spectral techniques etc. The synthesized compounds were screened for their biological activities and the result was compared with the standards

Open access

Direct determination of absolute stereochemistry of α-methylselenocysteine using the Mosher method

Robert J. Wehrle, Douglas R. Powell, Douglas S. Masterson

Article 100114

View PDF Article preview

Abstract

Abstract

Mosher amides of α-methylselenocysteine were synthesized to determine the absolute stereochemistry of the sterically hindered α-carbon utilizing ^{1}H, ^{13}C, ^{19}F, and ^{77}Se NMR spectroscopies. After analysis of these spectra using the established Mosher method, the stereochemistry of the α-carbon was determined to be (*R*), which was subsequently confirmed using x-ray crystallography.

Open access

Synthesis of “Click BOX” ligands and preliminary results on their application in the asymmetric copper catalysed Henry reaction of *o*-methoxybenzaldehyde

Daniela Giunta, Antonio Arras, Paola Peluso, Maurizio Solinas

Article 100122

View PDF Article preview

Abstract Graphical abstract

Graphical abstract

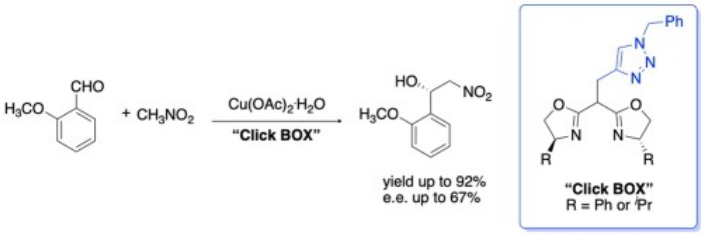

Open access

A convenient method for preparing the ionic Nickel (bis-dithiolene) complexes

Y.L. Wang, J.Y. Jia, D. Zhang, A.H. Han

Article 100130

View PDF Article preview

Abstract Graphical abstract

Graphical abstract

João Marcos Gomes de Oliveira Ferreira, Girlyanderson Araújo da Silva, Maisa Cavalcanti Coelho, Claudio Gabriel Lima Junior, Juliana Alves Vale

Article 100135

View PDF Article preview

Abstract

Abstract

A variety of knoevenagel compounds from isatin were synthesized using an eco-friendly methodology. It was used only the binary solvent ethanol: water (3:7 v/v) without the presence of metal catalyst what enabled the reaction between different isatins with malononitrile in a quick reaction time of 2–5 min and isolated yields 80–96%. When cyanoesters were used as methylene actives, the reactions were longer and the knoenevagel products were obtained 79–92% isolated yields.

Open access

Establishment of salicylic acid derived silylation reagents for protection of alcohols

Max Amann, Peter Fritz, Alexis Krupp, Stefan Heuser

Article 100139

View PDF Article preview

Abstract Graphical abstract

Graphical abstract

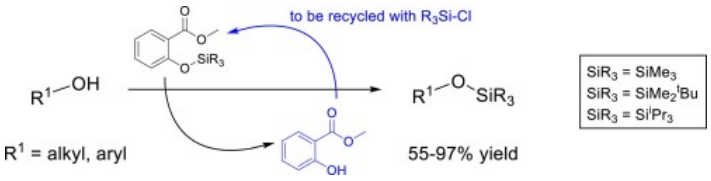

Open access

Synthesis, characterisation and DFT studies of [3,5-*bis*(2-hydroxyphenyl)-1*H*-1,2,4-triazol-1-yl](phenyl)methanone derivatives

Louis-Charl C. Coetzee, Alfred J. Muller, Adedapo S. Adeyinka, Molahlehi S. Sonopo, D. Bradley G. Williams

Article 100165

View PDF Article preview

Abstract Graphical abstract

Graphical abstract

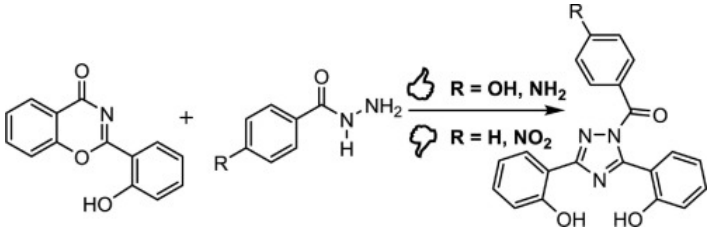

Open access

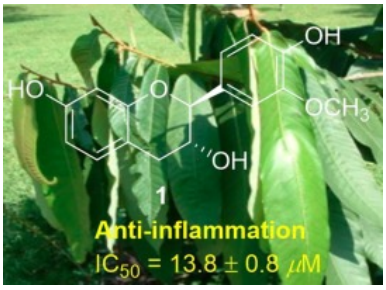

Medicinal Chemistry and Chemical Biology

Open access

Steps toward enhancing the fluorescence of small-molecule-based protein labels using supramolecular hosts

Pragati K. Prasad, Leila Motiei, David Margulies

Article 100134

View PDF Article preview

Abstract

Abstract

Labeling of proteins with small-molecule-based fluorescent probes provides a powerful tool to determine their expression level and localization in living cells. We propose a method for increasing and stabilizing the emission of such probes using supramolecular hosts such as β-cyclodextrin (β-CD). Although the emission of a His-tag binding probe was enhanced in the presence of β-CD, binding of the probe-β-CD complex to a His-tagged protein led to partial β-CD displacement and consequently, a reduction in the emission signal.

Review Article

Correspondence *Open access*

Convenient one-step synthesis of alkoxy substituted pyrazine derivatives

Yabin Song, Likun Xu, Baogang Wang, Dongna Zhang, Hongquan Wang

Article 100191

View PDF Article preview

Abstract

Abstract

We report a one-step method for the synthesis of alkoxy substituted pyrazine derivatives. The process makes use of an improved acid-mediated coupling reaction to afford the products in good yields (70–90%). This method expands the scope to alkoxy substituted pyrazine structures that are poorly represented in literature.

Review article *Open access*

$CoFe_2O_4/Cu(OH)_2$ Nanocomposite: Expeditious and magnetically recoverable heterogeneous catalyst for the four component Biginelli/transesterification reaction and their DFT studies

Anjaneyulu Bendi, G.B. Dharma Rao, Nutan Sharma, Manoj.P. Singh

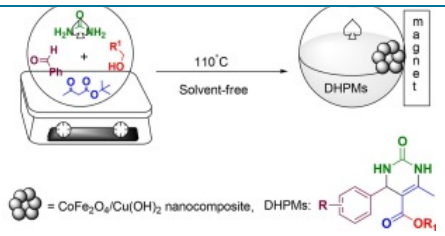

Organic Chemistry

Review article *Open access*

Easy access to both enantiomers of 5-hydroxyequol and 3-(4-hydroxyphenyl)chroman-8-ol

Takahito Uemura, Motohiro Sonoda, Shinji Tanimori

Article 100252

View PDF Article preview

Abstract Graphical abstract

Graphical abstract

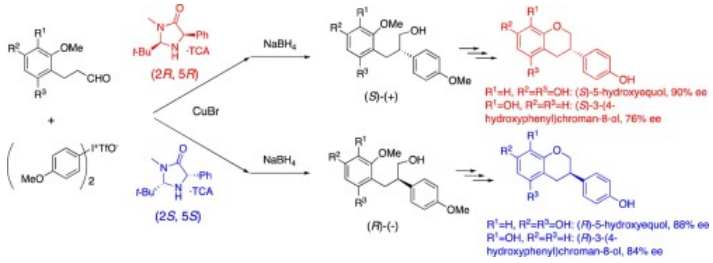

Inorganic Chemistry

Review article *Open access*

Bismuth sulfide based compounds: Properties, synthesis and applications

Timothy O. Ajiboye, Damian C. Onwudiwe

Article 100151

View PDF Article preview

Abstract

Abstract

Bismuth sulfide is one of the important compounds of bismuth that has garnered much attention due to its interesting properties and numerous applications. The structural orientation of bismuth sulfide and the characterization techniques have been highlighted. An in depth discussion were made on the various methods of synthesizing bismuth sulfide including chemical, sol–gel, deposition, pyrolysis, mechanical milling, microwave, microemulsion, Bridgman and successive ionic layer and reaction methods. Its medical applications, use in storage and generation of hydrogen, production of energy saving devices, as sensor for gas and other

Article 100138

View PDF Article preview

Abstract

Abstract

Developing robust methods to detect the severe acute respiratory syndromecoronavirus-2 (SARS-CoV-2), a causative agent for the current global health pandemic, is an exciting area of research. Nevertheless, the currently used conventional reverse transcription-polymerase chain reaction (RT-PCR) technique in COVID-19 detection endures with some inevitable limitations. Consequently, the establishment of rapid diagnostic tools and quick isolation of infected patients is highly essential. Furthermore, the requirement of point-of-care testing is the need of the hour. Considering this, we have provided a brief review of the use of very recently reported robust spectral tools for rapid COVID-19 detection. The spectral tools include, colorimetric reverse transcription loop-mediated isothermal amplification (RT-LAMP) and matrix-assisted laser desorption/ionization mass spectrometry (MALDI-MS), with the admittance of principal component analysis (PCA) and machine learning (ML) for meeting the high-throughput and fool-proof platforms for the detection of SARS-CoV-2, are reviewed. Recently, these techniques have been readily applied to screen a large number of suspected patients within a short period and they demonstrated higher sensitivity for the detection of COVID-19 patients from unaffected human subjects.

Medicinal Chemistry and Chemical Biology

Review article *Open access*

Biflavonoid as potential 3-chymotrypsin-like protease (3CLpro) inhibitor of SARS-Coronavirus

Yustina Hartini, Bakti Saputra, Bryan Wahono, Zerlinda Auw, ... Maywan Hariono

Article 100087

View PDF Article preview

Abstract

Abstract

3CL protease is one of the key proteins expressed by SARS-Coronavirus-2 cell, the potential to be targeted in the discovery of antivirus during this COVID-19 pandemic. This protein regulates the proteolysis of viral polypeptide essential in forming RNA virus. 3CL protease (3CLpro) was commonly targeted in the previous SARS-Coronavirus including bat and MERS, hence, by blocking this protein activity, the coronavirus should be eradicated. This study aims to review the potency of biflavonoid as the SARS-Coronavirus-2 3CLpro inhibitor. The review was initiated by describing the chemical structure of biflavonoid and followed by listing its natural source. Instead, the synthetic pathway of biflavonoid was also elaborated. The 3CLpro structure and its function were also illustrated followed by the list of its 3D-crystal structure available in a protein data bank. Lastly, the pharmacophores of biflavonoid have been identified as a protease inhibitor, was also discussed. This review hopefully will help researchers to obtain packed information about biflavonoid which could lead to the study in designing and discovering a novel SARS-Coronavirus-2 drug by targetting the 3CLpro enzyme.

Review article *Open access*

Antifungal constituents from *Nicotiana tabacum* with the *Wz* locus infected by *Phytophthora nicotianae*

Ying-Li Yang, Bi-Qing Song, Jing-Yu Long, Duan-Huang Fang, ... Yue-Hu Wang

Article 100196

View PDF Article preview

Abstract Graphical abstract

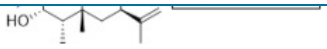

Others

Review article *Open access*

Graphene-supported nanomaterials as electrochemical sensors: A mini review

H.C. Ananda Murthy, Kiflom Gebremedhn Kelele, C.R. Ravikumar, H.P. Nagaswarupa, ... Tegene Desalegn

Article 100131

View PDF Article preview

Abstract

Abstract

Graphene has been a prominent choice as a base material for supporting varieties of inorganic and organic materials in scientific research and innovation due to its superior physico-chemical properties. Electrochemical sensors have been prepared by the use of a variety of nanoparticles and based on graphene which effectively supported on the surface of glassy carbon electrode through different methods. Graphene supported sensors have been utilized to detect and determine different electroactive species in samples. Many characterization techniques such as Powder X-ray diffraction (XRD), Energy dispersion spectroscopy (EDS), X-ray photoelectron spectroscopy (XPS), UV–Vis spectroscopy, Fourier transform infrared (FTIR) spectroscopy, Raman spectroscopy, High-resolution transmission electron microscopy (HRTEM), Scanning electron microscopy (SEM), transmission electron microscopy (TEM), and atomic force microscopy (AFM) have been successfully applied to explore the properties of graphene supported nanomaterials. Applications of the sensors have been assessed using signals from electrochemical measurements such as: cyclic voltammetry (CV), electrochemical impedance spectroscopy (EIS), and Differential pulse voltammetry (DPV). The results obtained from these measurements have data of wide liner range with small detection limit.

VSI:Inorg Bio Palaniandavar

Research article *Open access*

Molecular basis of quercetin as a plausible common denominator of macrophage-cholesterol-fenofibrate dependent potential COVID-19 treatment axis

Anil Pawar, Amit Pal, Kalyan Goswami, Rosanna Squitti, Mauro Rongiolettie

Article 100148

View PDF Article preview

Abstract

Abstract

The world's largest randomized control trial against COVID-19 using remdesivir, hydroxychloroquine, lopinavir and interferon-β1a appeared to have little or no effect on hospitalized COVID-19 patients. This has again led to search for alternate re-purposed drugs and/or effective “add-on” nutritional supplementation, which can complement or enhance the therapeutic effect of re-purposed drug. Focus has been shifted to therapeutic targets of severe acute respiratory syndrome coronavirus (SARS-CoV-2), which includes specific enzymes and regulators of lipid metabolism. Very recently, fenofibrate (cholesterol-lowering drug), suppressed the SARS-CoV-2 replication and pathogenesis by affecting the pathways of lipid metabolism in lung cells of COVID-19 patients. A preclinical study has shown synergistic effect of quercetin (a flavonoid) and fenofibrate in reducing the cholesterol content, which might be useful in COVID-19 treatment. Based on the scientific literature, use of quercetin and fenofibrate in COVID-19 seems meaningful in pharmaceutical and biomedical research, and warrants basic, experimental and clinical studies. In this article, we have summarized the contemporary findings about drug fenofibrate and its effect on membrane synthesis of COVID-19 virus along with emphasizing on possible synergistic effects of quercetin with fenofibrate.

View PDF Article preview

Abstract

Abstract

A library of palladium(II) acylthiourea complexes (**1**–**6**) of the type [$PdCl_2${$C_8H_{13}N_2OS(R)$}$_2$] [where R=$C_6H_4CH_3$(*o*) (**1**), C_6H_5 (**2**), $C_6H_4OCH_3$(*p*) (**3**), $C_6H_4OC_2H_5$(*p*) (**4**), $C_{10}H_7$ (**5**) or C_6H_5Cl(*p*) (**6**)] was synthesized and characterized by UV–Visible, FT-IR, ^{1}H NMR, ^{13}C NMR and ESI-Mass spectroscopy, and elemental analysis. Single crystal X-ray structure of complex **4** revealed the monodentate coordination of acylthiourea ligand through sulphur atom to the palladium ion in a *trans* fashion. In addition, variable-temperature (VT) NMR studies were performed to analyze the fluxional nature of complexes. The interaction of complexes with calf thymus (CT) DNA and BSA (bovine serum albumin) was analyzed by spectroscopic and molecular docking studies. The results inferred intercalation binding mode of the complexes with DNA. All the complexes exhibited good binding with BSA as well. Further, the complexes were found to act as good scavengers of DPPH as deduced from the antioxidant assay. *In vitro* cytotoxicity of the compounds against A549 (lung) cancer and HEK293 (human embryonic kidney) normal cell lines was investigated by MTT assay. Among the six complexes, complex **5** bearing a napthyl substitution in acylthiourea exhibited a remarkable activity against A549 cell line with an IC_{50} value of 14.8μM and was more active than cisplatin (IC_{50}=17.8μM). On the

Physical Chemistry and Chemical Physics

Review article *Open access*

Graphene synthesis, characterization and its applications: A review

Vestince B. Mbayachi, Euphrem Ndayiragije, Thirasara Sammani, Sunaina Taj, ... Atta ullah khan

Article 100163

View PDF Article preview

Abstract

Abstract

Since 2004, graphene has attracted a lot of attention among scientists and engineers. In recent years, graphene, a two dimensional monolayer planar sheet of sp^2-bonded carbon atom has witnessed a revolution in its applications because of its exemplary unique properties in terms of large specific surface area, physicochemical properties, mechanical strength, extraordinary thermal and electronic conductivity. There are several techniques used to synthesize high-quality graphene on a large scale. This review summarizes the fabrication of graphene by chemical, mechanical, thermal decomposition and chemical vapor deposition. In addition, the characterization methods and applications of graphene in different research fields have been discussed. This article winds up by giving a brief summary, illuminate the problems, and states the prospects of graphene.

supramolecular chemistry

Research article *Open access*

Development of metallosupramolecular phosphatases based on the combinatorial self-assembly of metal complexes and organic building blocks for the catalytic hydrolysis of phosphate monoesters

Shin Aoki, Akib Bin Rahman, Yosuke Hisamatsu, Yuya Miyazawa, ... Tomohiro Tanaka

Article 100133

View PDF Article preview

Abstract

assembly of different bis(Zn^{2+}-cyclen) complexes containing 2,2′-bipyridyl (bpy) linker (cyclen=1,4,7,10-tetraazacyclododecane), cyanuric acid or barbital (Bar) units, and Cu^{2+} ion in single or two-phase solvent systems. It is now thought that the appropriate combination of the various building blocks and solvent systems (single- and two-phase solvent systems) can strongly assist in developing the artificial systems that accelerate and catalyze the hydrolysis of a phosphate monoester, mono(*p*-nitrophenyl)

VSI:Recent Adv in org chem

Organic Chemistry

Research article *Open access*

Microwave assisted synthesis of phenanthridine derivatives via Suzuki coupling and condensation

Satheesh Kumar Dende, Raghu Babu Korupolu, Raju Doddipalla, Krishnakanth Reddy Leleti

Article 100149

View PDF Article preview

Abstract

Abstract

One-pot synthesis of phenanthridine derivatives using appropriately substituted aromatic *ortho*-bromo *N*-tosylhydrazones and 2′-aminobenzeneboronic acid pinacol esters is described. In the presence of Pd(amphos)Cl_2 catalyst, tosylhydrazone precursors undergo a Suzuki cross-coupling reaction with 2′-aminobenzeneboronic acid pinacol ester derivatives followed by intramolecular condensation to form the corresponding phenanthridines derivatives in one step.

Page 1 of 2

Previous vol/issue Next vol/issue

About this publication

ISSN: 2211-7156

Results in Chemistry 3 (2021) 100113

Contents lists available at ScienceDirect

Results in Chemistry

journal homepage: www.elsevier.com/locate/rechem

An integrated virtual screening of compounds from *Carica papaya* leaves against multiple protein targets of SARS-Coronavirus-2

Pandu Hariyono, Christine Patramurti, Damiana S. Candrasari, Maywan Hariono *

Faculty of Pharmacy, Sanata Dharma University, Campus III, Paingan, Maguwoharjo, Sleman 55282, Yogyakarta, Indonesia

ARTICLE INFO

Keywords:
ADMET prediction
Carica papaya
Coronavirus
COVID-19
Natural product
Virtual screening

ABSTRACT

The pandemic of SARS-Coronavirus-2 (Coronavirus-19) has been progressing by the increasing trend of the cases as well as deaths with neither vaccine nor drug is rationally used to stop the viral spread over. This study aims to perform an integrated virtual screening of compounds that had been identified from *Carica papaya* - leaves, which are proposed to be a herbal treatment for SARS-Coronavirus-2. The screening was initiated by evaluating the 40 compounds from *Carica papaya* leaves for their drug-like likeness property. The selected compounds were then secondly screened using carcinogenic and toxicity filters. Further selected compounds were thirdly screened for their pharmacokinetic profile and the screening was lastly performed by docking the third selected compounds against multiple protein targets of SARS-Coronavirus-2 employing 3-chymotrypsin-like protease (3CLpro), papain-like protease (PLpro), RNA-dependent-RNA-polymerase (RdRp), endonuclease (EndoU), S1 and S2 region of spike protein. The results show that 20 of 40 compounds, which meet the requirements of drug-like likeness, carcinogenicity-toxicity filter, and pharmacokinetic profiles, can interact with the multiple protein targets of SARS-Coronavirus-2 with the order from high to low affinity as follows: S1 > 3CLpro > EndoU > RdRp > PLpro > S2. In conclusion, *Carica papaya* leaves are worth to be proposed for further *in vitro* study against SARS-Coronavirus-2 at both molecular and cellular levels.

1. Introduction

The outbreak of severe acute respiratory syndrome (SARS) Coronavirus 2019 (Covid-19) has been extending across the world along with the number of victims. As reported by WHO in 6th November 2020, there had been 219 countries, 47,596,852 cases, and 1,216,357 deaths affected by the coronavirus [1]. The fast transmission from human to human-made the victims increase day by day without any specific antiviral agents being applied to the infected patients [2]. The treatment using HIV antiviral agent (lopinavir) [3], antimalaria (chloroquine) [4], and anti-influenza (oseltamivir) [5] have been a little bit helping the urgent situation, however, those could be still in trial and error since no selective drug has been discovered, up to now. Currently, remdesivir is an approved re-purposed drug from ebola and marburg antiviral agent to Coronavirus-19 which is indicated for adults and adolescents (12 years old or older) with body weight at least 40 kg [6]. The viral infection also could not be prevented since the vaccine is still under assessment [7]. Although China's Sinovac Biotech appeared to be safe in a late-stage clinical trial in Brazil, however, it still undergoes monitoring of the adverse side effects in the few months ahead [8].

The coronavirus is structurally made of an enveloped, positive sense, and single-stranded RNA that belongs to the family Coronaviridae [9]. Like many other coronaviruses (genera alpha, beta, and delta), the large replicase polyproteins pp1a and pp1ab are encoded by the partially overlapping 5′-terminal orf1a/b within the 5′ two-thirds of the genome is proteolytically cleaved into 16 putative nonstructural proteins (nsps) [10]. These putative nsps included two viral cysteine proteases, namely, nsp3 (papain-like protease) and nsp5 (chymotrypsin-like, 3C-like, or main protease), nsp12 (RNA-dependent RNA polymerase [RdRp]), nsp13 (helicase), and other nsps which are likely involved in the transcription and replication of the virus [9]. Other proteins of SARS-Coronavirus-2 that could be targeted are EndoU, S1, and S2. EndoU (nsp15) is a part of the SARS-Coronavirus-2 replicase-transcriptase system, responsible for virus replication and transcription system. S1 and S2 are regions of SARS-Coronavirus-2 spike protein that plays a key role in the receptor recognition and cell membrane fusion process. S1 domain can bind with human angiotensin-converting enzyme 2 (ACE2) receptor to initiate the fusion process by changing its conformation to pre-hairpin intermediate. This state enables the assembly of the fusion core in the S2 region of spike protein and

* Corresponding author.
E-mail address: mhariono@usd.ac.id (M. Hariono).

https://doi.org/10.1016/j.rechem.2021.100113
Received 18 November 2020; Accepted 11 February 2021

bringing viral and cellular membranes into proximity for membrane fusion [11].

To date, there is no clinically approved inhibitor of the SARS protease yet they remain in development [12]. The protease inhibitor for a diverse virus has been existing [13] such as nelfinavir [14], amprenavir for HIV [15], and lopinavir-ritonavir [16] for HCV. However, the production of those protease inhibitors required a multistep reaction which is very expensive, while we need an emergency drug that is effective, but not costly.

A study in the past time found that biflavonoid amentoflavone from *Torreya nucifera* showed significant inhibition towards SARS-Coronavirus 3CLpro with IC_{50} 8.3 μM. At the subsequent study, flavonoids including apigenin, luteolin, and quercetin also demonstrated IC_{50} 280.8, 20.2, and 23.8 μM, respectively, toward the protease proving that flavonoid is a potential scaffold for SARS-Coronavirus 3CLpro inhibitor [17]. Recently, flavonoid namely 5,6,7-trihydroxy-2-phenyl-4H-chromen-4-one (baicalein) has been co-crystallized with SARS-Coronavirus-2 3CLpro which confirmed the such compound's binding site with the protease [18].

Flavonoid is known to have a pleiotropic effect meaning that is not only a single protein that can be targeted but also can affect the multiple protein targets in the one disease pathogenesis [19]. On the other hand, RdRp is an essential protease that catalyzes the RNA replication while encoded in the genomes of all RNA-containing viruses with no DNA stage. A compound mimicking biflavonoid namely theaflavin was marked to suppress SARS-Coronavirus-2 replication through inhibiting RdRp [20].

Papaya (*Carica papaya*) is one of the tropical fruits known containing amino acid, protein, carbohydrate, fiber, vitamin C, and other nutrients [21]. In particular leaves, there are at least 40 compounds (Table S1) identified in which flavonoid and its analogs present approximately 27% [22–25]. These flavonoids and its analogs are including apigenin, catechin, deoxyquercetin, hesperitin, isorhamnetin, kaempferol, myricetin, naringenin, protocatechuic acid, quercetin, and rutin.

A molecular docking study had been conducted by Muhammad et al., presenting seven compounds from the whole *Carica papaya* trees against SARS-Coronavirus-2 3CLpro, PLpro, and RdRp [26]. In this present study, we performed *in silico* studies presenting 40 phytoconstituents of *Carica papaya* leaves against the two proteases (3CLpro and PLpro), RdRp, EndoU, S1, and S2 targeted protein of SARS-Coronavirus-2. The study was initiated by computationally screening those 40 compounds for their drug-like likeness, carcinogenicity-toxicity, and pharmacokinetics profiles using pkCSM online tools. The 20 hits from that were then simulated separately against 3CLpro, PLpro, RdRp, EndoU, S1, and S2 proteins of SARS-Coronavirus-2 using molecular docking.

2. Materials and methods

2.1. Materials

The protein model was using the SARS-Coronavirus-2 3D crystal structure of 3CLpro in complex with 5,6,7-trihydroxy-2-phenyl-4H-chromen-4-one with PDBID 6M2N [27], PLpro in complex with Ac-hTyr-Dap-Gly-Gly-VME (PDBID 6WX4) [28], RdRp in complex with cofactors (nsp7 and nsp8) (PDBID 6M71) [29], apo-EndoU (PDBID 6W01) [30], apo-S1 (PDBID 6VXX) [31], and apo-S2 (PDBID 6VSB) [32]. The 3D structure of the 40 ligands was downloaded from PubChem (https://pubchem.ncbi.nlm.nih.gov/). The software being used was Biovia Discovery Studio 2020 (www.accelrys.com), AutodockTools1.5.6 (www.scripps.edu), AutodockVina which is embedded in PyRx version 0.8 (https://pyrx.sourceforge.io/), and pkCSM online tool (http://biosig.unimelb.edu.au/pkcsm/prediction). The hardware is with specifications as followed: HP Notebook 14 CM-0006-AU, processor AMD Ryzen 3 2200AU, HDD 1 TB, RAM 4 GB, and OS Windows 10.

2.2. Methods

The *in silico* prediction was initiated by screening 40 compounds of *Carica papaya* leaves collected from the PubChem database using MW, LogP, followed by AMES test and lastly human gastrointestinal absorption. The final screened compounds were then simulated using molecular docking against 3CLpro, PLpro, RdRp, EndoU, S1 dan S2 (see Fig. 1).

2.3. Drug-like likeness study

Forty ligands were downloaded from https://pubchem.ncbi.nlm.nih.gov/ and converted into SMILES files. Its Lipinski Rule properties were individually predicted by inputting its SMILES string and the prediction was done by the server. Instead of molecular weight and LogP were the filter representing the drug-like likeness, there are a few more parameters in this study including the number of hydrogen bond donor (HBD), the number of hydrogen bond acceptor (HBA), the number of rotatable bonds and the surface area, were also predicted.

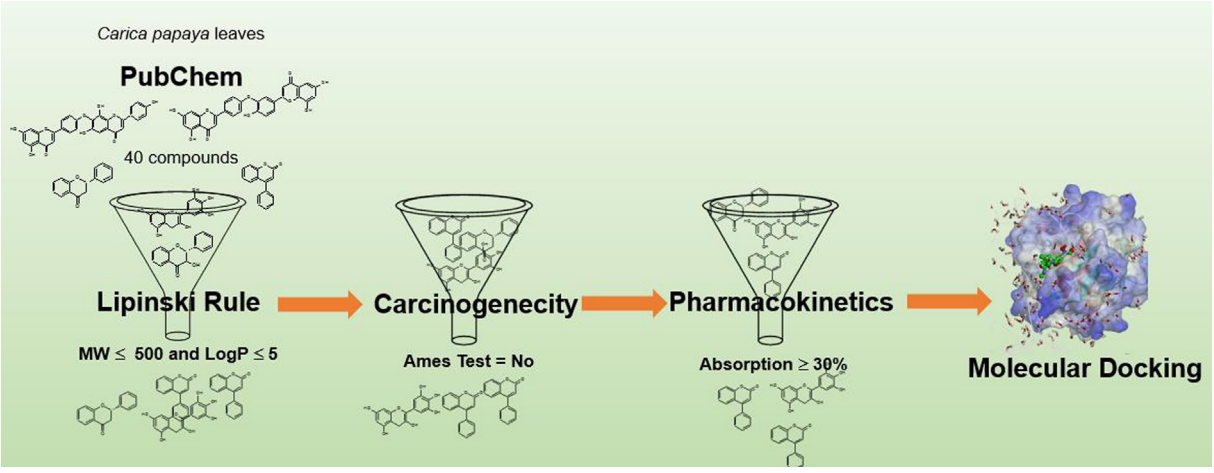

Fig. 1. The screening steps of 40 compounds from *Carica papaya* leaves in identifying the potential of this leaves to be a natural source for combating SARS-Coronavirus-2.

2.4. Carcinogenic and toxicity studies

Using the same protocol in section 2.1, the carcinogenic profile of the selected compounds was represented by the AMES test result. Instead, other parameters such as maximum tolerated dose (human) (hMTD), hERG I inhibitor, hERG II inhibitor, oral rat acute toxicity (LD_{50}), oral rat chronic toxicity (LOAEL), hepatotoxicity, skin sensitization, *T. pyriformis* toxicity, and minnow toxicity.

2.5. Pharmacokinetics study

Using the same protocol in 2.2, the pharmacokinetic profiles (absorption, distribution, metabolism, and excretion) of the selected compounds were used as the filter. Subsequently, the absorption is influenced by water solubility, Caco2 permeability, skin permeability, P-glycoprotein substrate, P-glycoprotein I inhibitor, and P-glycoprotein II inhibitor, instead of human gastrointestinal absorption. The distribution is represented by VDss (human), fraction unbound (human), blood–brain barrier (BBB) permeability, and central nervous system (CNS) permeability. The metabolism is represented by the CYP2D6 substrate, CYP3A4 substrate, CYP1A2 inhibitor, CYP2C19 inhibitor, CYP2C9 inhibitor, CYP2D6 inhibitor, and CYP3A4 inhibitor. Lastly, the excretion is represented by total clearance and renal OCT2 substrate.

2.6. Molecular docking study

2.6.1. Protein preparation

The 3D protein crystal structures were downloaded from www.rcsb.org and then uploaded in Discovery Studio. The complexed ligand from the individual protein target was taken out from the complex and the protein was saved as pdb file. The pdb protein file was then uploaded into Autodocktools1.5.6 and added by polar hydrogen followed by giving Kollman charge. The protein was then saved as pdbqt and ready for use.

3. Ligand preparation

The ligand for control docking was prepared by uploading it to AutodockTools1.5.6, given polar and non-polar hydrogen, Gasteiger charge and then saved as pdbqt. The available ligands in PubChem database (https://pubchem.ncbi.nlm.nih.gov/) were directly downloaded in its 3D structure followed by uploading them into Discovery Studio and then saved as pdb file. The optimized structure in PubChem server was reported in the published paper [33,34]. Each pdb ligands were then uploaded into Autodocktools1.5.6 and then given gasteiger charges. The ligands were then saved as pdbqt and ready for use.

3.0.1. Control docking

The control docking was carried by redocking the individual native ligand into the respecting protein target with the parameters as followed: gridbox size ($25 \times 25 \times 25$) with the center of mass x = –33.718, y = −65.831, z = 41.2267; x = 9.4133, y = −28.3762, z = −38.0803; and x = 113.1457, y = 115.4740, z = 125.2150, for 3CLpro, PLpro, RdRp. The coordinate ligand being docked into EndoU, S1 and S2, respectively: x = 113.146, y = 115.474, z = 125.2150; x = 228.417, y = 208.3656, z = 256.074; and x = 203.530, y = 239.600 z = 186.327. The docking was run using Autodock Vina embedded in PyRx program with exhaustiveness = 64 covering 9 conformations for each ligand. The binding energy result was collected in csv file, whereas the best docking pose was selected and saved in pdbqt file ready for analysis. The control docking parameters were accepted when the RMSD value was not greater than 2.0 Å [35].

3.0.2. Virtual screening

The virtual screening through molecular docking of 20 ligands against 3CLpro, PLpro and RdRp, EndoU, S1, and S2 spike proteins of SARS-Coronavirus-2 was carried out using the same procedure of the individual control docking.

3.0.3. Analysis

The ligands were ranked according to the binding energy from the lowest to the highest value. Ten top lowest free energies of binding were then selected as the virtual hits. These virtual hits were then analyzed its molecular interaction with the binding site of the individual protein target using Discovery Studio 2020.

4. Results

The drug-like likeness is one of the criteria for a compound to be a drug candidate. This is well-known with the Lipinski Rule of Five postulating that a drug should be maximum having 500 g/mol in the molecular weight, <5 in the partition coefficient (log P), maximum of 5 in the number of hydrogen bond donor (HBD), and lastly maximum of 10 in the number of hydrogen bond acceptor (HBA) [36]. This rule is not 100% ensuring, however, it is guiding the drug design process. The log P is the ratio of the concentration of the compound in *n*-octanol over its concentration in water, therefore it associates with the balance of the compound's solubility in water during oral dissolution steps with its oral bioavailability of the compound in the blood system [36]. The log P < 5 is estimated to be the ideal value when the compound dissolves in our body fluid as well as its absorption through the gastrointestinal cell membrane, and then to be transported into the blood system. In this study, the first filter of 40 compounds from *Carica papaya* leaves was shortlisting 31 compounds having the maximum logP value less than 5 (Table S2). The second filter was, 23 of them passed the carcinogenicity effect by showing non-responsive toward the AMES test (Table S3). Finally, 20 compounds having at least 30% gastrointestinal absorption as the 3rd filter were shortlisted. Table 1 presents the 20 final selected compounds having log P are less than 5 along with other Lipinski Rule of Five criteria.

A drug should have MW which is lower than 500 Da, log P < 5, the number of HBD ≤ 5, the number of HBA ≤ 10, rotatable bonds ≤10, and surface area ≤140 Å [36,37]. MW will affect the potency of the drug which is commonly expressed in IC_{50}. The higher of MW would be the lower IC_{50}, therefore, the more potent the drug. However, the MW should not be greater than 500 considering the drug permeability during intestinal absorption [36]. The number of HBD or HBA reflects their polarity to interact with water during the dissolution process as well as their molecular interaction during the pharmacodynamic step [36]. The rotatable bonds may influence their stability during pharmacokinetics and the receptor binding, thus, the less rotatable chain in the molecule should be the more stable drug to perform their activity [36,37]. The polar surface area (SA) associates with the permeability of drugs across the cell membrane in which the higher SA might be poorer in cell permeability (oral bioavailability) [36,37]. Therefore, catechin, deoxyquercetin, and deoxykaempferol are among compounds which meet the Lipinski rule for drug-like likeness.

A physical or chemical agent that exposes to an individual by causing cancer is named carcinogen, which in some carcinogenic agents, they are associated with increasing the risk of developing specific types of cancer [38]. For example, construction workers that are frequently exposed to asbestos, a carcinogenic agent, have been strongly linked to the development of a specific type of lung cancer called mesothelioma [39]. Importantly, it was identified some carcinogens from drug bearing phenacetin and azathioprine structures [40]. Table 2

Table 1
The drug-like likeness profile of 20 compounds selected from *Carica papaya* leaves.

Ligands	Lipinski Rule				Rotatable Bonds	Surface area
	MW	log P	HBD	HBA		
2*S*-sambunigrin	295.291	−0.93222	4	7	4	121.142
5,7-dimethoxycoumarin	206.197	1.8102	0	4	2	86.036
anthraquinone	208.216	2.462	0	2	0	92.536
apigenin	270.24	2.5768	3	5	1	112.519
ascorbic acid	176.124	−1.4074	4	6	2	67.321
caffeic acid	180.159	1.1956	3	3	2	74.381
caffeoyl alcohol	166.176	1.1033	3	3	2	70.219
catechin	290.271	1.5461	5	6	1	119.662
deoxykaempferol	270.24	2.5768	3	5	1	112.519
deoxyquercetin	286.239	2.2824	4	6	1	117.313
dimethoxyphenol	154.165	1.4094	1	3	2	65.183
ferulic acid	194.186	1.4986	2	3	3	81.065
kaempferol	286.239	2.2824	4	6	1	117.313
niacin	123.111	0.7798	1	2	1	51.972
p-coumaric acid	164.16	1.49	2	2	2	69.587
p-coumaroyl alcohol	150.177	1.3977	2	2	2	65.425
protocatechuic acid	154.121	0.796	3	3	1	62.341
riboflavin	376.369	−1.72356	5	9	5	152.292
R-prunasin	295.291	−0.93222	4	7	4	121.142
thiamine	265.362	0.60774	2	5	4	109.957

Table 2
The AMES test result of the 20 final selected compounds for carcinogenicity prediction along with other toxicity profiles.

Ligands	Toxicity									
	AMES*	hMTD	hERG I **	hERG II **	LD_{50}	LOAEL	Hepato*	SS	Tp*	Minnow*
2*S*-sambunigrin	No	1.117	No	No	2.714	3.316	No	No	0.285	3.396
5,7-dimethoxycoumarin	No	0.711	No	No	2.137	2.59	No	No	0.609	1.06
anthraquinone	No	0.083	No	No	2.316	2.2	No	Yes	0.922	0.514
apigenin	No	0.83	No	Yes	2.423	1.753	No	No	0.386	1.114
ascorbic acid	No	1.987	No	No	1.434	3.376	No	No	0.285	3.612
caffeic acid	No	0.326	No	No	1.992	2.028	No	No	0.034	1.587
caffeoyl alcohol	No	0.289	No	No	1.994	1.959	No	Yes	0.326	1.941
catechin	No	1.072	No	No	2.261	3.212	No	No	0.285	1.833
deoxykaempferol	No	0.479	No	No	2.428	1.977	No	No	0.474	1.536
deoxyquercetin	No	0.837	No	No	2.651	1.592	No	No	0.304	1.263
dimethoxyphenol	No	1.345	No	No	1.809	2.866	No	No	0.252	1.212
ferulic acid	No	0.475	No	No	2.076	3.046	No	No	−0.011	1.492
kaempferol	No	0.676	No	No	2.698	1.658	No	No	0.3	1.407
niacin	No	1.168	No	No	2.008	2.862	No	No	−0.446	2.329
p-coumaric acid	No	0.338	No	No	2.099	2.908	No	No	0.01	1.739
p-coumaroyl alcohol	No	0.729	No	No	2.117	2.08	No	Yes	0.033	2.118
protocatechuic acid	No	0.607	No	No	1.951	2.341	No	No	−0.136	1.955
riboflavin	No	0.509	No	No	1.91	3.81	Yes	No	0.285	3.828
R-prunasin	No	1.117	No	No	2.714	3.316	No	No	0.285	3.396
thiamine	No	0.238	No	No	2.635	1.204	Yes	No	0.247	2.599

* = toxicity; ** = inhibitor

presents the AMES test result of the 20 final selected compounds for carcinogenicity prediction along with other toxicity profiles.

Toxicity predictions are used to predict whether these compounds having dangerous or toxic properties towards human physiology. AMES toxicity is employed to assess compounds carcinogenicity/mutagenic properties, therefore drug candidates should not be mutagenic or carcinogenic [38,41]. The human maximum tolerated dose (hMTD) used to predict the value of the toxic dose threshold in human with the value of log hMTD for more than 0.477, are considered to be acceptable. hERG I and II are potassium channels that mediate the repolarizing of a cardiac action potential in humans. Inhibition of these proteins is the main cause of long QT syndrome development that might lead to fatal arrhythmia, hence drugs should not inhibit these ion channels. LD_{50} value represents the value of the dose given to cause 50% death of a group of rats and shows toxic potency of a compound in which a higher value of LD_{50} is considered to be safer. LOAEL (lowest-observed-adverse-effect level) value shows the lowest concentration of a compound to cause an adverse effect in human physiology indicated by the alteration of morphology, function, growth, or development. The safety of a compound improves as the LOAEL value increases. Hepatotoxicity shows the toxicity of a compound to cause liver injuries which disrupt its functions. It is expected that drug candidates should be non-hepatotoxic as considered to be a major safety factor in drug development. Potential dermal adverse effects are tested using a skin sensitization test, thus a compound should not induce allergic skin dermatitis. *T. pyriformis* and minnow toxicity are both utilized to measure the value of toxic endpoints. Drug environment safety is now taken into account to reduce the environmental damage by drugs with the acceptable value of *T. pyriformis* and minnow toxicity to be respectively higher than 0.5 and −0.3. Based on the overall toxicity predictions, 2*S*-sambunigrin, catechin, deoxyquercetin, dimethoxyphenol, and *R*-prunasin are considered to have the best safety profiles among 20 compounds (http://biosig.unimelb.edu.au/pkcsm/prediction).

Before entering the binding site of the receptor, the drug will undergo pharmacokinetic steps including absorption, distribution,

metabolism, and excretion (ADME) [42]. The molecule should be absorbed from the gastrointestinal into the blood vessel through the lipid bilayer membrane reflecting its bioavailability. Next, the molecule will be distributed by the blood and further carried out into the targetted cell bearing the receptor, while being interrupted by the plasma-protein binding. Some drugs will have the first pass effect by the liver's enzymes which are early metabolized into either active or inactive drugs. Upon the receptor binding, the drug will give the therapeutic effect while gradually be metabolized by cytochrome P450 big family into their inactive metabolites. These metabolism products will be excreted throughout the body. Therefore, the prediction of pharmacokinetics profiles before docking using the software will help to design a compound that in one hand meets the ADME criteria, and on the other hand, it has a good binding with the receptor. Tables 3–5 and Fig. 2 present the pharmacokinetics profile of 20 hits selected from 40 compounds identified from the *Carica papaya* leaves using pkCSM online tool.

According to Table 3, 17 compounds demonstrate more than 50% human intestinal absorption, in which 5,7-dimethoxycoumarin, anthraquinone, apigenin, deoxykaempferol, dimethoxyphenol, ferulic acid, *p*-coumaric acid, *p*-coumaroyl alcohol, and thiamine are among having the best absorption profile for more than 90%. The drug properties should have water solubility represented as log S value is higher than −4, therefore, all compounds are predicted among the good drug properties during the dissolution step. Caco2 is also the *in vitro* cell model to predict the absorption of an orally administered drug [43]. The drug should have Caco2-permeability for more than 0.90, thus, only eight compounds are predicted to have a high human gastrointestinal absorption. For a transdermal route of administration, a compound should have a skin permeability for at least −2.5 or lower. Among 20 compounds, 18 of them are suitable for a transdermal dosage form (excluding 5,7-dimethoxycoumarin and anthraquinone). P-glycoprotein (P-gp) is a protein transport essential during pharmacokinetics steps. This could have either advantage in therapeutic effect or even the contradictive ones [44]. A compound should have no P-gp inhibition for either P-gp I or P-gp II. Therefore, no compounds are predicted to either slow down the therapeutic effect or its contraindication. In conjunction, this should be proportional with their P-gp substrate inhibition profiles.

During the distribution, a drug should have a steady state uniform concentration while reaching up the whole tissues rather than plasma [45]. This is defined by the number of VDss ≥ −0.15. Among 20 compounds, 8 compounds (anthraquinone, caffeoyl alcohol, catechin, deoxykaempferol, deoxyquercetin, dimethoxyphenol, *p*-coumaroyl alcohol and thiamine) are the ones which meet this criteria. Fraction unbound describes the amount of drug which is free from plasma protein binding associated with the total concentration ready for the receptor binding. This should have the value of ≥0.15, therefore, except antraquinone, apigenin, deoxykaempferol, and deoxyquercetin, the remained compounds are available for the receptor binding which may increase the drug activity. The BBB permeability defines the possibility of compound to cross the brain membrane which may affect the CNS [46]. For a safe drug, these values should be < −1 and < −3 (poorly distributed to the brain and unable to penetrate CNS) for BBB and CNS permeability, respectively. Therefore, compounds like 5,7-dimethoxycoumarin and anthraquinone should be taken in a good control to avoid the CNS either depression or excitation. Table 4 presents the distribution profile of 20 compounds identified in *Carica papaya* leaves.

Drug metabolism occurs mainly in the liver which will undergo chemical alteration to improve its excretion or elimination. There are main six subfamilies (CYPs) that are being responsible for most of human drug metabolism with CYP1A2, CYP2C9, CYP2C19, CYP2D6, CYP3A4, are some of the most important within these subfamilies [47]. CYP2D6 and CYP3A4 are the most significant enzymes in overall drug metabolism, and they are also found in extrahepatic sites such as in the brain for CYP2D6, which is responsible for drug activity in the brain. Other example is CYP3A4 in the intestines which is mainly affecting oral bioavailability by first-pass metabolism. Lower bioavailability and activity are expected for compounds that have a high affinity towards both enzymes as substrate. CYP450 enzymes activity can be modified by drugs, either inhibition or activation. This is potentially causing clinical drug-drug interactions, leading to adverse reactions or therapeutic failures. Therefore, inhibition of these enzymes increases the possibility of adverse drug reactions and interactions. Most likely, all compounds do not act as the substrate for CYP2D6 and CYP3A4, except anthraquinone which may act as the substrate of CYP3A4. More compounds are likely inhibit the CYP1A2 but less inhibit other CYP as shown in Table 5.

Drug excretion is a process of either eliminating or removing drugs directly in unchanged form or its inactive form. Most drugs are excreted by the kidneys and drug excretion becomes less efficient

Table 3
The absorption profiles of the 20 final selected compounds as predicted by the software.

Ligands	Absorption						
	Water solubility (log S)	Caco2 permeability	Intestinal absorption (human)	Skin Permeability	P-gp substrate	P-gp I inhibitor	P-gp II inhibitor
2*S*-sambunigrin	−3.574	0.212	40.072	−2.744	No	No	No
5,7-dimethoxycoumarin	−3.343	1.281	99.221	−2.401	No	No	No
anthraquinone	−2.387	1.041	99.925	−2.365	Yes	No	No
apigenin	−2.079	1.136	91.403	−2.736	Yes	No	No
ascorbic acid	−0.429	−0.395	39.716	−3.478	No	No	No
caffeic acid	−1.773	−0.046	55.525	−2.735	Yes	No	No
caffeoyl alcohol	−1.538	1.091	68.137	−3.047	Yes	No	No
catechin	−2.910	−0.225	62.740	−2.735	Yes	No	No
deoxykaempferol	−3.405	1.139	92.943	−2.735	Yes	No	No
deoxyquercetin	−2.987	0.109	84.972	−2.735	Yes	No	No
dimethoxyphenol	−2.101	0.841	95.368	−2.504	No	No	No
ferulic acid	−1.719	0.100	94.737	−2.709	Yes	No	No
kaempferol	−2.986	−0.053	84.952	−2.735	Yes	No	No
niacin	−0.515	1.219	86.389	−2.790	No	No	No
p-coumaric acid	−1.610	1.142	93.183	−2.566	Yes	No	No
p-coumaroyl alcohol	−1.325	1.491	92.284	−2.815	Yes	No	No
protocatechuic acid	−1.675	0.805	67.889	−2.736	Yes	No	No
riboflavin	−1.952	−0.385	54.626	−2.740	Yes	No	No
R-prunasin	−2.079	0.212	40.072	−2.744	No	No	No
thiamine	−2.903	0.872	92.302	−2.963	No	No	No

Table 4
The distribution profile of 20 compounds identified in *Carica papaya* leaves as predicted by the software.

Ligands	Distribution			
	log VDss (human)	Fraction unbound (human)	BBB permeability (log BB)	CNS permeability (log PS)
2*S*-sambunigrin	−0.706	0.439	−0.929	−4.57
5,7-dimethoxycoumarin	−0.141	0.37	0.274	−2.405
anthraquinone	0.251	0.118	0.252	−1.474
apigenin	−0.361	0.143	−1.082	−2.195
ascorbic acid	−0.264	0.808	−1.233	−4.332
caffeic acid	−0.409	0.358	−0.851	−3.326
caffeoyl alcohol	0.011	0.514	−0.347	−2.526
catechin	0.675	0.187	−1.182	−3.449
deoxykaempferol	0.354	0.148	−0.864	−2.092
deoxyquercetin	0.141	0.112	−1.219	−2.378
dimethoxyphenol	−0.112	0.486	−0.133	−2.092
ferulic acid	−0.535	0.397	−0.263	−2.93
kaempferol	−0.178	0.087	−1.361	−2.357
niacin	−0.794	0.601	−0.353	−2.928
p-coumaric acid	−0.602	0.421	−0.234	−2.379
p-coumaroyl alcohol	0.124	0.464	−0.183	−1.835
protocatechuic acid	−0.332	0.373	−0.985	−3.333
riboflavin	−0.818	0.558	−1.743	−5.243
R-prunasin	−0.706	0.439	−0.929	−4.57
thiamine	0.474	0.574	−0.441	−3.022

Table 5
The interaction between 20 ligands identified from *Carica papaya* leaves with a diverse CYP subfaimilies.

Parameter	Metabolism						
	CYP2D6 substrate	CYP3A4 substrate	CYP1A2 inhibitor	CYP2C19 inhibitor	CYP2C9 inhibitor	CYP2D6 inhibitor	CYP3A4 inhibitor
2*S*-sambunigrin	No	No	No	No	No	No	No
5,7-dimethoxycoumarin	No	No	Yes	No	No	No	No
anthraquinone	No	Yes	Yes	No	No	No	No
apigenin	No	No	Yes	Yes	Yes	No	Yes
ascorbic acid	No	No	No	No	No	No	No
caffeic acid	No	No	No	No	No	No	No
caffeoyl alcohol	No	No	No	No	No	No	No
catechin	No	No	No	No	No	No	No
deoxykaempferol	No	No	Yes	Yes	Yes	No	No
deoxyquercetin	No	No	Yes	No	Yes	No	Yes
dimethoxyphenol	No	No	Yes	No	No	No	No
ferulic acid	No	No	No	No	No	No	No
kaempferol	No	No	Yes	No	Yes	No	No
niacin	No	No	No	No	No	No	No
p-coumaric acid	No	No	No	No	No	No	No
p-coumaroyl alcohol	No	No	Yes	No	No	No	No
protocatechuic acid	No	No	No	No	No	No	No
riboflavin	No	No	No	No	No	No	No
R-prunasin	No	No	No	No	No	No	No
thiamine	No	No	Yes	No	No	No	No

and dosing adjustments may be needed as kidney function declines. Total clearance is the rate at which a compound is removed from the body i.e. excreted in the urine as a compound with a higher clearance value leads to shorter half-time and hence its effective duration [42]. Thiamine is the fastest compound to be eliminated from the body due to its highest total clearance. In contrast, caffeoyl alcohol is the slowest compound to be eliminated from the body due to its lowest total clearance.

Drugs may be passively excreted by the kidney through glomerular filtration or actively by tubular secretion. OCT2 transporter is one of the main renal uptake transporter to actively remove drug from blood. It plays a key role in the removal and renal clearance of mostly cationic drugs and endogenous compounds [48]. Inhibition of OCT2 (such as by cimetidine) decreases OCT2-dependent renal clearance drugs, such as metformin, hence altering pharmacokinetics and pharmacodynamics profiles that may lead to undesireable adverse effects. Interestingly, none compounds having inhibition towards renal OCT2 substrate that might be not having undesirable side effects. Based on the prediction, every ligands excretion will not depend on the renal OCT2 transporter.

The control docking results for 3CLpro and PLpro against their co-crystallized ligands are considered to be acceptable with a RMSD value of its internal ligand being 0.7146 Å and 1.2141 Å, respectively. On the other hand, the other proteins have no co-crystallized ligand, therefore, in this case, no control docking has been carried out for internal validation. However, we tried to do an external validation using remdesivir as this drug is primarily targetting RdRp, Glisoxepide for EndoU [49], *N*-(9,10-dioxo-9,10-dihydroanthracene-2-yl)benzamide for S1 spike protein [50], and captopril for S2 spike protein [51] of SARS-Coronavirus-2. PyRx has a facility to be a site finder that predicts the binding site of apoprotein. The binding affinity of remdisivir into RdRp SARS-Coronavirus-2 is −6.6 kcal/mol (catalytic site), and −8.6 kcal/mol (allosteric site) representing that the parameters are capable to calculate the binding affinity of the selected 20 compounds from *Carica papaya* leaves. Table S4 presents the control docking results of 3CLpro, PLpro, RdRp, EndoU, S1 dan S2 protein. At the same time, control docking of glisoxepide (EndoU), N-(9,10-dioxo-9,10-dihydroanthracene-2-yl)benzamide (S1 spike), and captopril (S2 spike) demonstrate the binding affinity of the ligand into the

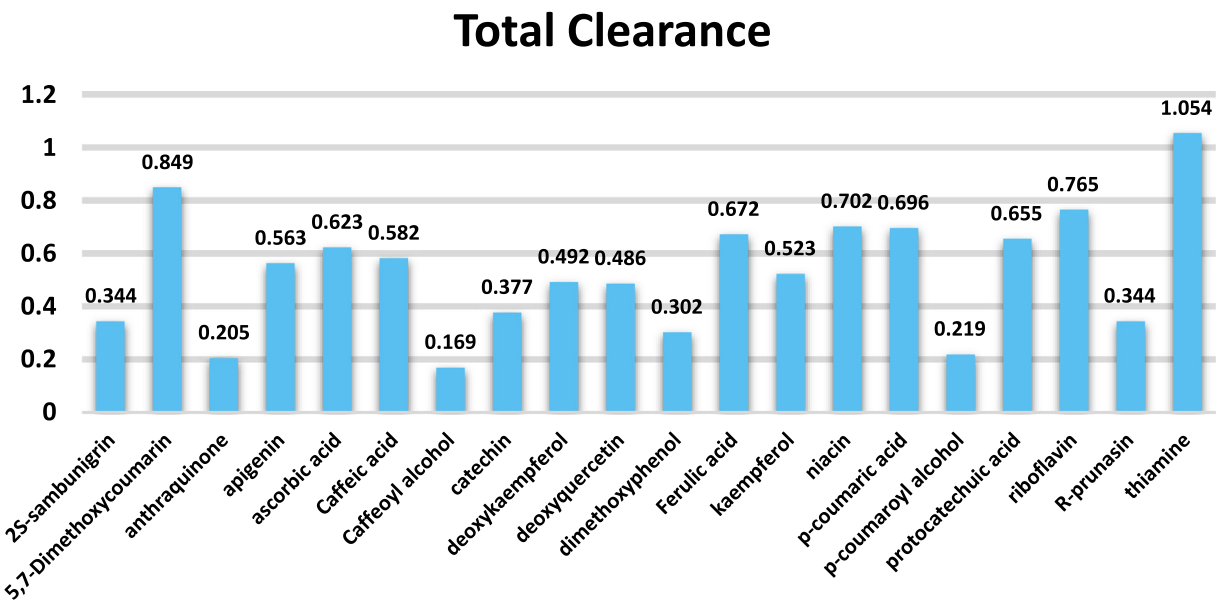

Fig. 2. The histogram plot of 20 compounds identified from *Carica papaya* leaves against their total clearance.

corresponding target as follows: −8.2, −9.7, and −4.5 kcal/ mol, respectively. Table 6 lists down the binding affinity of the selected 20 compounds from *Carica papaya* leaves.

From the docking results, 20 ligands show affinity with 3CLpro, PLpro, RdRp, EndoU, S1 and S2 ranging in −4.5 to −7.8 kcal/mol, −4.6 to −7.5 kcal/mol, −4.6 to −6.9 kcal/mol, −4.6 to −7.7 kcal/-mol, −4.9 to −8.2 kcal/mol, and −4.2 to −6.3 kcal/mol, respectively. These describe the most favorable interactions of the 20 ligands are to 3CLpro, EndoU, and S1, rather than PLpro, RdRp, and S2. This is in agreement with the average of the binding affinity, in which interaction with 3CLpro (−6.3 kcal/mol), EndoU (−6.1 kcal/-mol), and S1 (−6.6 kcal/mol) has the lowest binding energy as mentioned in parentheses. Fig. 3 illustrates the overlapping 20 ligands docked conformation in the binding site of individual 3CLpro, PLpro, RdRp, EndoU, S1, and S2.

In particular, on one hand, dexoyquercetin demonstrates the lowest binding energy toward 3CLpro (-7.8 kcal/mol), whereas catechin performed the most favorable binding toward EndoU. Furthermore, kaempferol shows the lowest binding energy toward S1 (-8.2 kcal/mol). On the other hand, riboflavin, kaempferol, and apigenin demonstrate the lowest binding energy towards PLpro, RdRp and S2, respectively. Figs. 4 and 5 illustrates the best binding pose of ligands into individual protein binding sites.

The binding pose of deoxyquercetin in the 3CLpro binding site occurs through the H-bond interaction with GLU166 and PHE140. Instead, the ligand pose might be stabilized by the hydrophobic interaction with HIS163, MET165, and GLU166. In the binding pose of riboflavin in PLpro binding site, the H-bond interaction occurred at ASP302, VAL165, ARG166, TYR273, and SER245, whereas the hydrophobic interactions were performed by interacting with

Table 6
The binding affinity of 20 compounds identified from *Carica papaya* leaves upon molecular docking study into 3CLpro, Plpro, RdRp, EndoU, S1 and S2 spike of SARS-Coronavirus-2.

Ligands	Binding Affinity (Kcal/mol)					
	3CLpro	PLpro	RdRP	EndoU	S1	S2
2*S*-sambunigrin	−7.0	−6.0	−6.5	−6.5	−7.3	−5.3
5,7-dimethoxycoumarin	−5.8	−5.9	−5.4	−5.4	−6.1	−5.4
anthraquinone	−6.5	−5.7	−6.4	−6.8	−7.0	−5.9
apigenin	−7.2	−6.6	−6.5	−7.2	−7.7	−6.3
ascorbic acid	−5.0	−4.9	−5.4	−4.7	−5.6	−4.8
caffeic acid	−5.8	−5.2	−5.7	−6.1	−6.1	−4.9
caffeoyl alcohol	−5.4	−4.9	−5.1	−6	−5.9	−4.8
catechin	−7.5	−6.3	−6.9	−7.7	−7.8	−6.1
deoxykaempferol	−7.4	−6.8	−6.5	−7.2	−7.8	−6.0
deoxyquercetin	−7.8	−6.7	−6.7	−7.5	−8.0	−6.0
dimethoxyphenol	−4.7	−4.4	−4.7	−5.7	−4.9	−4.2
ferulic acid	−5.6	−5.2	−5.4	−5.7	−6.1	−4.8
kaempferol	−7.2	−6.7	−6.9	−7.2	−8.2	−5.9
niacin	−4.5	−4.6	−4.6	−4.6	−4.9	−4.7
p-coumaric acid	−5.3	−4.8	−5.2	−5.6	−5.9	−4.6
p-coumaroyl alcohol	−5.0	−4.7	−4.7	−5.2	−5.3	−4.4
protocatechuic acid	−5.1	−4.9	−5.6	−5.1	−5.8	−4.6
riboflavin	−7.4	−7.5	−6.6	−6.6	−8.1	−6.2
R-prunasin	−6.8	−6.1	−6.3	−6.6	−7.1	−5.6
thiamine	−5.8	−6.1	−6.0	−5.3	−7.0	−5.1
Mean	−6.3	−5.7	−5.9	−6.1	−6.6	−5.3

S1, and S2.

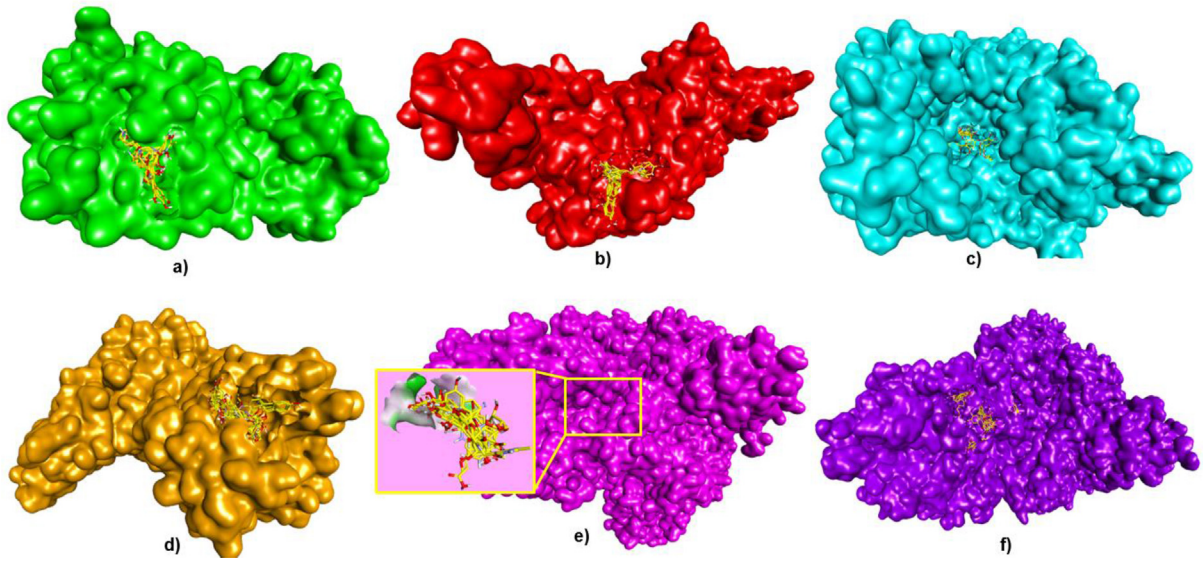

Fig. 3. The overlapping docked pose of 20 compounds identified from *Carica papaya* leaves in the binding site of a) 3CLpro, b) PLpro, c) RdRp, d) EndoU, e) S1, and f) S2. The proteins were presented in a surface model, whereas the ligands were presented in a yellow stick model, with C, H, O, and N are colored by yellow, white, red and blue, respectively. (For interpretation of the references to colour in this figure legend, the reader is referred to the web version of this article.)

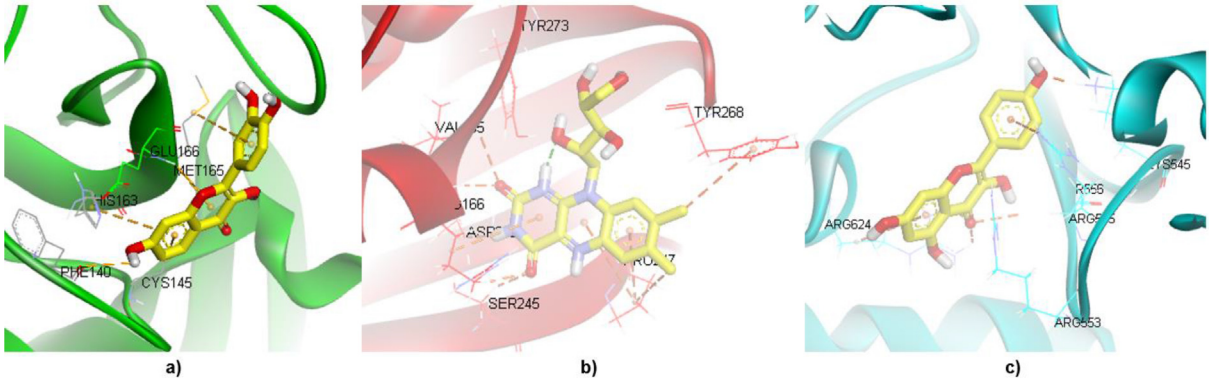

Fig. 4. The docking pose of a) deoxyquercetin (−7.8 kcal/mol) into 3CLpro, b) riboflavin into PLpro (−7.5 kcal/mol), and c) kaempferol (−6.9 kcal/mol) into RdRp. The proteins were visualized in ribbon model, whereas the ligands were presented in a yellow stick model, with C, H, O, and N are colored by yellow, white, red and blue, respectively. The H-bond interaction and the hydrophobic interaction are presented in black and orange dashed lines, respectively. (For interpretation of the references to colour in this figure legend, the reader is referred to the web version of this article.)

PRO247, TYR268, and ARG166. Kaempferol interacts with LYS545, THR556, ARG553, and ARG624. The hydrophobic interactions of this complex occur at the residues identical to H-bond interactions.

The H-bond interactions were further shown by catechin while interacting with HIS250, ASN278, LYS290, SER294, and LEU346 of EndoU. Besides, the hydrophobic interactions were performed by interacting with TYR343 and LYS345. Kaempferol was again showing the best affinity with SER371, ARG408, and GLN409 of S1 protein. The only hydrophobic interaction was performed by interacting with PRO384. S2 protein binding site was occupied by apigenin in its best binding affinity among 20 ligands performing H-bond interactions with LYS933, THR719, SER929, and ALA930. There is no hydrophobic interaction identified in this binding pose. The detail information about distance and angle of individual H-bond interactions is presented in Table 7. H-bonds can be classified into weak, moderate and strong H-bonds depending on its angle and distance. Strong H-bonds have the distance range from 2.2 to 2.5 Å and angle between 170 and 180 degree, whereas weak H-bonds have the distance more than 3.2 Å and the angle more than 90 degree. Moderate H-bonds have the distance between strong and weak H-bonds and the angle more than 130 degree [52].

5. Discussion

Carica papaya leaves have been traditionally used to relieve dengue fever in some Asian countries. The leaves are sliced into smaller pieces and followed by boiling them into the water for at least 15 min and then filtered out to collect the liquid phase. This 30 mL of the aqueous extract is three times daily used for dengue patients until the fever fully recovered into a normal body temperature [53].

Scientifically, the methanolic extract of *Carica papaya* leaves showed cytotoxic effects (CC_{50} = 0.6156 mg/mL) to LLC-MK2 cells and it showed inhibitory activity ($EC_{50} \geq 1$ mg/mL) against DENV-2 with a selectivity index value of $\pm > 1$ [54]. Treatments with 500 mg/kg and 1000 mg/kg of freeze-dried *Carica papaya* leaf juice

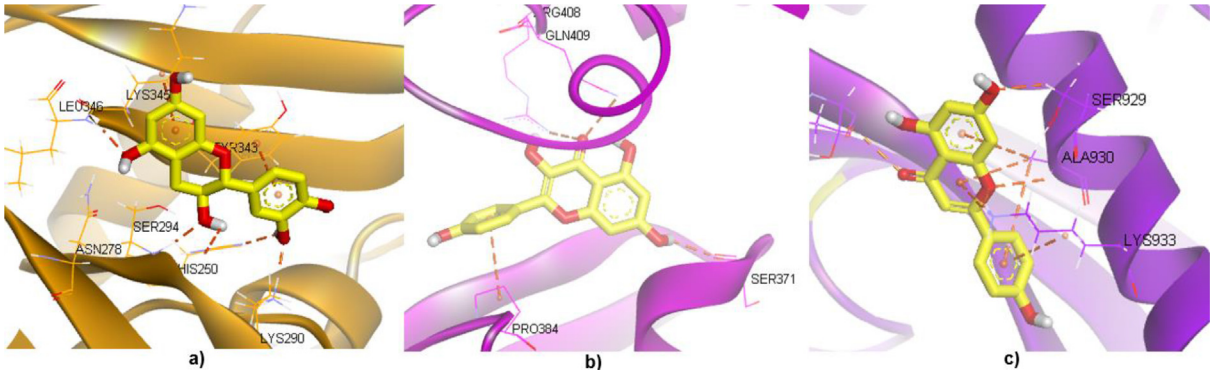

Fig. 5. The docking pose of a) catechin (−7.7 kcal/mol) into EndoU, b) kaempferol into S1 (−8.2 kcal/mol), and c) apigenin (−6.3 kcal/mol) into S2. The proteins were visualized in ribbon model, whereas the ligands were presented in a yellow stick model, with C, H, O, and N are colored by yellow, white, red and blue, respectively. The H-bond interaction and the hydrophobic interaction are presented in black and orange dashed lines, respectively. (For interpretation of the references to colour in this figure legend, the reader is referred to the web version of this article.)

Table 7
The detail information about distance and angle of individual H-bond interactions. The atom type and numbering of each ligands are defined in Table S5.

Targets	Ligands	Interactions	HB distance (Å)	HB angles (°)	Remark
Mpro	deoxyquercetin	GLU166:NH – DOQ:O1	2.235	152.940	Moderate
		DOQ:H29 – PHE140:O	2.929	91.570	Weak
PLpro	riboflavin	VAL165:NH – RF:O6	3.050	117.750	Weak
		ARG166:NH – RF:O6	2.317	159.880	Moderate
		TYR273:H – RF:N9	2.667	92.620	Weak
		RF:H46 – ASP302:OD1	2.323	144.660	Moderate
		SER245:HB2 – RF:O5	2.567	143.085	Moderate
RdRp	kaempferol	LYS545:HZ3 – KF:06	1.970	167.720	Moderate
		THR556:HG1 – KF:O4	2.910	115.190	Weak
		ARG624:HH12 - KF:O4	2.367	107.920	Weak
		ARG624:HH22 - KF:O4	2.283	108.620	Weak
EndoU	catechin	LYS290:HZ3 – CTC:O5	1.960	172.756	Strong
		SER294:NH – CTC:O2	2.042	160.573	Moderate
		LEU346:NH – CTC:O3	2.108	154.170	Moderate
		CTC:H34 – HIS250:NE2	2.312	129.033	Weak
		ASN278:HD22 – CTC:O3	2.208	137.886	Moderate
S1	kaempferol	GLN409:HE21 – KF:O4	2.820	94.092	Weak
		ARG408:HH12 – KF:O2	2.336	135.509	Moderate
		ARG408:HH22 – KF:O2	2.247	137.850	Moderate
S2	apigenin	LYS933:HZ3 – APG:O1	2.225	147.531	Moderate
		THR719:HB – APG:O3	2.615	136.176	Moderate
		SER929:HB2 – APG:O4	2.548	119.748	Weak
		ALA930:HA – APG:O1	2.892	132.931	Moderate

increased the platelet and leukocyte counts in DENV2-infected AG129 mice. A significant decrease ($p < 0.05$) in viral RNA level was detected in the liver and kidney of infected AG129 mice treated with 1000 mg/kg of freeze-dried *Carica papaya* leaf juice. *Carica papaya* treatment also significantly decreased ($p < 0.05$) the levels of certain cytokines and chemokines in plasma, liver, and kidney tissues of infected AG129 mice [55]. A study by Sharma et al. suggested that papaya leaves extract significantly decreases the expression of the envelope and NS1 proteins in DENV-infected THP-1 cells. This marked a decrease in intracellular viral load upon the extract treatment confirmed its antiviral activity [56].

Studies were carried out on natural papain inhibitor from papaya latex. The isolated fractions, identified as inhibitors I and II, showed a negative reaction with ninhydrin; however, the fraction identified as P-III showed a positive reaction with ninhydrin. Kinetics data showed non-competitive inhibition (inhibitor I) and uncompetitive (inhibitors II and P-III) [57]. *In silico* anti-dengue activities of the extracts from *Carica papaya* by using bioinformatics tools were investigated. Interestingly, the flavonoid quercetin performed the highest binding energy against NS2B-NS3 protease which is evidenced by the formation of six hydrogen bonds with the amino acid residues at the binding site of the receptor [58]. This is then later proven by *in vitro* study, that flavonoid quercetin able to inhibit the DENV2 NS2B-NS3 protease through a non-competitive inhibition [59]

In this present study, an integrated *in silico* screening has been performed against 40 compounds identified from *Carica papaya* leaves. The 40 compounds have a diverse scaffold bearing flavonoid, flavanol, alkaloid, phytosterol, glycoside, phenylpropanoid, carbohydrate, coumarin, anthraquinone, and flavin class compounds. These compounds have their drug-like likeness, carcinogenicity, toxicity, pharmacokinetics, and pharmacodynamic profiles that contribute to the therapeutic effect of *Carica papaya* leaves as discussed above. There had been 20 of those 40 compounds finally selected, which might contribute to the therapeutic effects better than its toxic properties.

These 20 compounds were predicted to meet the rule of Lipinski, therefore, they should be stable during oral administration. These selected compounds should not be carcinogenic, cardiotoxic, hepatotoxic, and having drug tolerance that lowering the drug safety index. These compounds also should be well absorbed by the biological membrane and then well distributed into the site of action. Upon therapeutic effects, these compounds should be easily metabolized into an inactive metabolite and followed by the excretion of chemicals from

our body system to minimize chemical retention that could be having adverse drug reactions. Finally, these 20 compounds demonstrated molecular interactions upon *in silico* docking them into the diverse protein targets of SARS-Coronavirus-2. According to the binding energy average, the 20 compounds interact with the protein in a sequence of higher to lower binding affinity as follows: S1 > 3CLpro > EndoU > RdRp > PLpro > S2. This means that most likely, *Carica papaya* might disrupt the SARS-Coronavirus-2 life cycle by interrupting the binding of spike protein into ACE2 receptor, the proteolysis of nsp4-13, and the reverse RNA transcription rather than inhibiting the RNA replication, proteolysis of nsp1-3, and the fusion core in S2 region of spike protein and bringing viral and cellular membranes into proximity for membrane fusion.

The notable compounds' performance in their protein target is most likely having flavonoid/ flavanol/ flavin scaffold. This is for sure in correspondence with the previous studies that flavonoid class compound has a pleiotropic effect upon biological targets. By blocking the S1 protein binding to its ACE2 receptor, flavonoids in *Carica papaya* may contribute to its prevention toward the SARS-Coronavirus cell invasion. The immunomodulatory effects of *Carica papaya* leaves may also work on the target, therefore, this is in agreement with the study by Norahmad et al. The second hypothesis on how the *Carica papaya* leaves would eradicate the SARS-Coronavirus-2 cell proliferation is by blocking the 3CLpro enzymatic activity. This is proven by the therapeutic effect of flavonoid quercetin to inhibit DENV2 NS2B-NS3 protease which is also a serine protease enzyme as studied by de Sousa et al [60,61].

The *in silico* structure-based drug design has been applied in this study to speed up the discovery of SARS-Coronavirus-2 antiviral agents using an inexpensive and rational approach [62,63]. *Carica papaya* is a natural product which is a highly available and abundant resource that could lead for an effective and efficient herbal drug [64] to combat SARS-Coronavirus-2 pandemic.

6. Conclusion

In conclusion, *Carica papaya* leaves have the potential to be the SARS-Coronavirus-2 antiviral agent from herbal. This is due to the 20 compounds presenting in its leaves which have drug-like likeness structure, non-carcinogenic, non-toxic, pharmacokinetically and pharmacodynamically stable as predicted by *in silico* experiments. The major flavonoid compounds that are interacting with a diverse protein target of SARS-Coronavirus-2, could be the rational reason on how this herbal would be promising as this antiviral agent.

CRediT authorship contribution statement

Pandu Hariyono: Investigation, Conceptualization. **Christine Patramurti:** Writing - review & editing. **Damiana S. Candrasari:** Writing - review & editing. **Maywan Hariono:** Conceptualization, Writing - review & editing.

Declaration of Competing Interest

The authors declare that they have no known competing financial interests or personal relationships that could have appeared to influence the work reported in this paper.

Acknowledgements

We greatly acknowledge to National Center for Biotechnology Information (NCBI), Dassault Systemes BIOVIA, Scripps Research, and Bio21 Institute University of Melbourne for freely providing PubChem (https://pubchem.ncbi.nlm.nih.gov/), Discovery Studio 2020 (www.accelrys.com), AutodockTools1.5.6 (www.scripps.edu) and Autodock-Vina which is embedded in PyRx version 0.8 (https://pyrx.sourceforge.io/), and pkCSM online tool (http://biosig.unimelb.edu.au/pkcsm/prediction).

Funding

This work was supported by the Lembaga Penelitian and Pengabdian Masyarakat (LPPM) of Sanata Dharma University [No. 039/LPPM USD/V/2020] under Covid-19 Research Grant Special Theme.

Appendix A. Supplementary data

Supplementary data to this article can be found online at https://doi.org/10.1016/j.rechem.2021.100113.

References

[1] World Health Organization 2020, World Health Organization official website, 6 November 2020 <https://www.who.int/emergencies/diseases/novel-coronavirus-2019>.
[2] H.A. Rothan, S.N. Byrareddy, The epidemiology and pathogenesis of coronavirus disease (COVID-19) outbreak, J. Autoimmun. 109 (February) (2020), https://doi.org/10.1016/j.jaut.2020.102433 102433.
[3] A.R. Sahin, 2019 Novel Coronavirus (COVID-19) outbreak: a review of the current literature, Eurasian J. Med. Oncol. 4 (1) (2020) 1–7, https://doi.org/10.14744/ejmo.2020.12220.
[4] C.C. Lai, T.P. Shih, W.C. Ko, H.J. Tang, P.R. Hsueh, Severe acute respiratory syndrome coronavirus 2 (SARS-CoV-2) and coronavirus disease-2019 (COVID-19): the epidemic and the challenges, Int. J. Antimicrob. Agents 55 (3) (2020), https://doi.org/10.1016/j.ijantimicag.2020.105924 105924.
[5] V. Letchumanan, N.-S. Ab Mutalib, B.-H. Goh, L.-H. Lee, Novel coronavirus 2019-nCoV: could this virus become a possible global pandemic, Progr. Microbes Mol. Biol. 3 (1) (2020) 1–6, https://doi.org/10.36877/pmmb.a0000068.
[6] Drugs.com 2020, Drugs.com official website, 30 October 2020 <https://www.drugs.com/history/veklury.html>.
[7] S. Jiang, L. Du, Z. Shi, An emerging coronavirus causing pneumonia outbreak in Wuhan, China: calling for developing therapeutic and prophylactic strategies, Emerging Microbes Infect. 9 (1) (2020) 275–277, https://doi.org/10.1080/22221751.2020.1723441.
[8] Al Jazeera 2020, Al Jazeera English official website, 11 November 2020 https://www.aljazeera.com/news/2020/11/10/brazil-halts-trials-of-chinese-covid-19-vaccine.
[9] J.F.W. Chan, K.H. Kok, Z. Zhu, H. Chu, K.K.W. To, S. Yuan, K.Y. Yuen, Genomic characterization of the 2019 novel human-pathogenic coronavirus isolated from a patient with atypical pneumonia after visiting Wuhan, Emerging Microbes Infect. 9 (1) (2020) 221–236, https://doi.org/10.1080/22221751.2020.1719902.
[10] D. Paraskevis, E.G. Kostaki, G. Magiorkinis, G. Panayiotakopoulos, G. Sourvinos, S. Tsiodras, Full-genome evolutionary analysis of the novel corona virus (2019-nCoV) rejects the hypothesis of emergence as a result of a recent recombination event, Infection, Genetics Evol. 79 (January) (2020), https://doi.org/10.1016/j.apsb.2020.02.008 104212.
[11] C. Wu, Y. Liu, Y. Yang, P. Zhang, W. Zhong, Y. Wang, Q. Wang, Y. Xu, M. Li, X. Li, M. Zheng, L. Chen, H. Li, Analysis of therapeutic targets for SARS-CoV-2 and discovery of potential drugs by computational methods, Acta Pharm. Sinica B 10 (5) (2020) 766–788, https://doi.org/10.1016/j.apsb.2020.02.008.
[12] Stoermer, M., 2020. Homology Models of Coronavirus 2019-nCoronavirus 3CLpro Protease.
[13] R. Vardanyan, V. Hruby, Synthesis of Best-Seller Drugs, Academic Press, 2016.
[14] J.J. Gills, J. LoPiccolo, J. Tsurutani, R.H. Shoemaker, C.J.M. Best, M.S. Abu-Asab, J. Borojerdi, N.A. Warfel, E.R. Gardner, M. Danish, M.C. Hollander, S. Kawabata, M. Tsokos, W.D. Figg, P.S. Steeg, P.A. Dennis, Nelfinavir, a lead HIV protease inhibitor, is a broad-spectrum, anticancer agent that induces endoplasmic reticulum stress, autophagy, and apoptosis in vitro and invivo, Clin. Cancer Res. 13 (17) (2007) 5183–5194, https://doi.org/10.1158/1078-0432.CCR-07-0161.
[15] A.G. Marcelin, C. Lamotte, C. Delaugerre, N. Ktorza, H.A. Mohand, R. Cacace, M. Bonmarchand, M. Wirden, A. Simon, P. Bossi, F. Bricaire, D. Costagliola, C. Katlama, G. Peytavin, V. Calvez, Genotypic inhibitory quotient as predictor of virological response to ritonavir-amprenavir in human immunodeficiency virus type 1 protease inhibitor-experienced patients, Antimicrob. Agents Chemother. 47 (2) (2003) 594–600, https://doi.org/10.1128/AAC.47.2.594-600.2003.
[16] X. Sáez-Llorens, A. Violari, C.O. Deetz, R.A. Rode, P. Gomez, E. Handelsman, S. Pelton, O. Ramilo, P. Cahn, E. Chadwick, U. Allen, S. Arpadi, M.M. Castrejón, R.S. Heuser, D.J. Kempf, R.J. Bertz, A.F. Hsu, B. Bernstein, C.L. Renz, E. Sun, Forty-eight-week evaluation of lopinavir/ritonavir, a new protease inhibitor, in human immunodeficiency virus-infected children, Pediatric Inf. Dis. J. 22 (3) (2003) 216–223, https://doi.org/10.1097/01.inf.0000055061.97567.34.
[17] Y.B. Ryu, H.J. Jeong, J.H. Kim, Y.M. Kim, J.Y. Park, D. Kim, T.T.H. Naguyen, S.J. Park, J.S. Chang, K.H. Park, M.C. Rho, W.S. Lee, Biflavonoids from Torreya nucifera displaying SARS-CoV 3CLpro inhibition, Bioorg. Med. Chem. 18 (22) (2010) 7940–7947, https://doi.org/10.1016/j.bmc.2010.09.035.

[18] H.X. Su, S. Yao, W.F. Zhao, M.J. Li, L.K. Zhang, Y. Ye, Y.C. Xu, 2020. Identification of a novel inhibitor of SARS-Coronavirus-2 3CLpro. published online, 10.

[19] G.L. Russo, M. Russo, C. Spagnuolo, The pleiotropic flavonoid quercetin: from its metabolism to the inhibition of protein kinases in chronic lymphocytic leukemia, Food Funct. 5 (10) (2014) 2393–2401, https://doi.org/10.1039/c4fo00413b.

[20] J. Lung, Y.S. Lin, Y.H. Yang, Y.L. Chou, L.H. Shu, Y.C. Cheng, H.T. Liu, C.Y. Wu, The potential chemical structure of anti-SARS-CoV-2 RNA-dependent RNA polymerase, J. Med. Virol. 92 (6) (2020) 693–697, https://doi.org/10.1002/jmv.25761.

[21] V. Yogiraj, P.K. Goyal, C.S. Chauhan, A. Goyal, B. Vyas, Carica papaya Linn: an overview, Int. J. Herbal Med. 2 (5 Part A) (2014) 1–8.

[22] A. Canini, D. Alesiani, G. D'Arcangelo, P. Tagliatesta, Gas chromatography-mass spectrometry analysis of phenolic compounds from Carica papaya L. leaf, J. Food Comp. Anal. 20 (7) (2007) 584–590, https://doi.org/10.1016/j.jfca.2007.03.009.

[23] S. Akhila, N.G. Vijayalakshmi, Phytochemical studies on carica papaya leaf juice, Int. J. Pharm. Sci. Res. 6 (2) (2015) 880–883.

[24] A. Nugroho, H. Heryani, J.S. Choi, H.J. Park, Identification and quantification of flavonoids in Carica papaya leaf and peroxynitrite-scavenging activity, Asian Pacific J. Trop. Biomed. 7 (3) (2017) 208–213, https://doi.org/10.1016/j.apjtb.2016.12.009.

[25] M. Kaur, N.C. Talniya, S. Sahrawat, A. Kumar, E.E. Stashenko, Ethnomedicinal uses, phytochemistry and pharmacology of carica papaya plant: a compendious review, Mini-Rev. Org. Chem. 16 (5) (2018) 463–480, https://doi.org/10.2174/1570193x15666180816110733.

[26] Muhammad, Y., Shehu, Z., Iliya, S., Bk, M., Ya, K., Mb, A., Wali, U., Yeldu, M.H., Tahiru, A., Ay, A., Yakubu, A., Habeeb, A., Ib, F., Sa, S., and Uf, A., 2020. Molecular Docking, Drug-Likeness and ADMET Analysis of Potential Inhibitors (Ligands) from Carica papaya Against Severe Acute Respiratory Syndrome Coronavirus 2 (SARS-CoV-2), 3389 (May), 222–232. 10.36348/sjm.2020.v05i05.00.

[27] Su, H. xia, Yao, S., Zhao, W. feng, Li, M. jun, Liu, J., Shang, W. juan, Xie, H., Ke, C. qiang, Hu, H. chen, Gao, M. na, Yu, K. qian, Liu, H., Shen, J. shan, Tang, W., Zhang, L. ke, Xiao, G. fu, Ni, L., Wang, D. wen, Zuo, J. ping, Jiang, H. liang, Bai, F., Wu, Y., Ye, Y., and Xu, Y. chun, 2020. Anti-SARS-CoV-2 activities in vitro of Shuanghuanglian preparations and bioactive ingredients. Acta Pharmacologica Sinica, 41 (9), 1167–1177. 10.1038/s41401-020-0483-6.

[28] W. Rut, Z. Lv, M. Zmudzinski, S. Patchett, D. Nayak, S.J. Snipas, F. El Oualid, T.T. Huang, M. Bekes, M. Drag, S.K. Olsen, Activity profiling and crystal structures of inhibitor-bound SARS-CoV-2 papain-like protease: a framework for anti–COVID-19 drug design, Sci. Adv. 6 (42) (2020) eabd4596, https://doi.org/10.1126/sciadv.abd4596.

[29] Y. Gao, L. Yan, Y. Huang, F. Liu, Y. Zhao, L. Cao, T. Wang, Q. Sun, Z. Ming, L. Zhang, J. Ge, L. Zheng, Y. Zhang, H. Wang, Y. Zhu, C. Zhu, T. Hu, T. Hua, B. Zhang, X. Yang, J. Li, H. Yang, Z. Liu, W. Xu, L.W. Guddat, Q. Wang, Z. Lou, Z. Rao, Structure of the RNA-dependent RNA polymerase from COVID-19 virus, Science 368 (6492) (2020) 779–782.

[30] Y. Kim, R. Jedrzejczak, N.I. Maltseva, M. Wilamowski, M. Endres, A. Godzik, K. Michalska, A. Joachimiak, Crystal structure of Nsp15 endoribonuclease NendoU from SARS-CoV-2, Protein Sci. 29 (7) (2020) 1596–1605, https://doi.org/10.1002/pro.3873.

[31] A.C. Walls, Y.J. Park, M.A. Tortorici, A. Wall, A.T. McGuire, D. Veesler, Structure, function, and antigenicity of the SARS-CoV-2 spike glycoprotein, Cell 181 (2) (2020) 281–292.e6, https://doi.org/10.1016/j.cell.2020.02.058.

[32] D. Wrapp, N. Wang, K.S. Corbett, J.A. Goldsmith, C.-L. Hsieh, O. Abiona, B.S. Graham, J.S. McLellan, Cryo-EM structure of the 2019-nCoV spike in the prefusion conformation, Science 367 (6483) (2020) 1260–1263, https://doi.org/10.1126/science.abb2507.

[33] D. Wang, Z. Li, Y. Liu, An overview of the safety, clinical application and antiviral research of the COVID-19 therapeutics, J. Inf. Public Health 13 (10) (2020) 1405–1414, https://doi.org/10.1016/j.jiph.2020.07.004.

[34] E.E. Bolton, J. Chen, S. Kim, L. Han, S. He, W. Shi, V. Simonyan, Y. Sun, P.A. Thiessen, J. Wang, B. Yu, J. Zhang, S.H. Bryant, PubChem3D: a new resource for scientists, J. Cheminf. 3 (1) (2011) 32, https://doi.org/10.1186/1758-2946-3-32.

[35] S.J. De Vries, M. Van Dijk, A.M.J.J. Bonvin, The HADDOCK web server for data-driven biomolecular docking, Nat. Protoc. 5 (5) (2010) 883–897, https://doi.org/10.1038/nprot.2010.32.

[36] C.A. Lipinski, Drug-like properties and the causes of poor solubility and poor permeability, J. Pharmacol. Toxicol. Methods 44 (1) (2000) 235–249, https://doi.org/10.1016/S1056-8719(00)00107-6.

[37] J.D. Armstrong, R.E. Hubbard, T. Farrell, B. Maiguashca, Structure-Based Drug Discovery: An Overview, Royal Society of Chemistry, 2006.

[38] E. Huerta, N. Grey, 2007. Cancer Control Opportunities in Low- and Middle-income Countries. CA: A Cancer J. Clin., 10.3322/canjclin.57.2.72.

[39] M. Uguen, J.-D. Dewitte, P. Marcorelles, B. Loddé, R. Pougnet, P. Saliou, M. De Braekeleer, A. Uguen, Asbestos-related lung cancers: a retrospective clinical and pathological study, Mol. Clin. Oncol. 7 (1) (2017) 135–139, https://doi.org/10.3892/mco.2017.1277.

[40] IARC Working Group on the Evaluation of Carcinogenic Risks to Humans, 2012. Pharmaceuticals. Volume 100 A. A review of human carcinogens. IARC monographs on the evaluation of carcinogenic risks to humans, 100 (Pt A), 1–401.

[41] McCormick, D.L., 2017. Preclinical Evaluation of Carcinogenicity Using Standard-Bred and Genetically Engineered Rodent Models. Second Edi. A Comprehensive Guide to Toxicology in Nonclinical Drug Development. Elsevier Inc. 10.1016/b978-0-12-803620-4.00012-8.

[42] S.E. Rosenbaum, 2016. Basic Pharmacokinetics and Pharmacodynamics, an Integrated Textbook and Computer Simulations, 2nd edition. 10.1111/j.1365-2125.2011.04077.x

[43] I. de Angelis, L. Turco, Caco-2 cells as a model for intestinal absorption, Curr. Protocols Toxicol. (SUPPL.47) (2011) 1–15.

[44] J.H. Lin, M. Yamazaki, Role of P-glycoprotein in pharmacokinetics, Clin. Pharmacokinet. 42 (1) (2003) 59–98, https://doi.org/10.2165/00003088-200342010-00003.

[45] C.J. Hull, Pharmacokinetics and pharmacodynamics, Br. J. Anaesth. 51 (1979) 579.

[46] P. Ballabh, A. Braun, M. Nedergaard, The blood-brain barrier: an overview: Structure, regulation, and clinical implications, Neurobiol. Dis. 16 (1) (2004) 1–13.

[47] M.T. Kinirons, M.S. O'Mahony, Drug metabolism and ageing, Br. J. Clin. Pharmacol. 57 (5) (2004) 540–544, https://doi.org/10.1111/j.1365-2125.2004.02096.x.

[48] H.J. Burt, S. Neuhoff, L. Almond, L. Gaohua, M.D. Harwood, M. Jamei, A. Rostami-Hodjegan, G.T. Tucker, K. Rowland-Yeo, Metformin and cimetidine: physiologically based pharmacokinetic modelling to investigate transporter mediated drug-drug interactions, Eur. J. Pharm. Sci. 88 (2016) 70–82, https://doi.org/10.1016/j.ejps.2016.03.020.

[49] A. Chandra, V. Gurjar, I. Qamar, N. Singh, Identification of potential inhibitors of SARS-COV-2 endoribonuclease (EndoU) from FDA approved drugs: a drug repurposing approach to find therapeutics for COVID-19, J. Biomol. Struct. Dyn. (2020) 1–11.

[50] A.O. Adedeji, W. Severson, C. Jonsson, K. Singh, S.R. Weiss, S.G. Sarafianos, Novel inhibitors of severe acute respiratory syndrome coronavirus entry that act by three distinct mechanisms, J. Virol. 87 (14) (2013) 8017–8028.

[51] B. Robson, CORONAVIRUS-19 Coronavirus spike protein analysis for synthetic vaccines, a peptidomimetic antagonist, and therapeutic drugs, and analysis of a proposed achilles' heel conserved region to minimize probability of escape mutations and drug resistance, Comput. Biol. Med. (2020). 103749.

[52] T. Steiner, The hydrogen bond in the solid state, Angew. Chem. Int. Ed. 41 (1) (2002) 48–76, https://doi.org/10.1002/1521-3773(20020104)41:1<48::AID-ANIE48>3.0.CO;2-U.

[53] S.A.M. Kularatne, Dengue fever, BMJ (Online) 351 (September) (2015) 1–10, https://doi.org/10.1136/bmj.h4661.

[54] B. Joseph, P. Sankarganesh, K. Ichiyama, N. Yamamoto, In vitro study on cytotoxic effect and anti-DENV2 activity of Carica papaya L. leaf, Front. Life Sci. 8 (1) (2015) 18–22, https://doi.org/10.1080/21553769.2014.924080.

[55] N.A. Norahmad, M.R. Mohd Abd Razak, N. Mohmad Misnan, N.H. Md Jelas, U.R. Sastu, A. Muhammad, T.C.D. Ho, B. Jusoh, N.A. Zolkifli, R. Thayan, A. Mat Ripen, M. Zainol, A.F. Syed Mohamed, Effect of freeze-dried Carica papaya leaf juice on inflammatory cytokines production during dengue virus infection in AG129 mice, BMC Compl. Alternative Med. 19 (1) (2019) 1–10, https://doi.org/10.1186/s12906-019-2438-3.

[56] N. Sharma, K.P. Mishra, S. Chanda, V. Bhardwaj, H. Tanwar, L. Ganju, B. Kumar, S. B. Singh, Evaluation of anti-dengue activity of Carica papaya aqueous leaf extract and its role in platelet augmentation, Arch. Virol. 164 (4) (2019) 1095–1110, https://doi.org/10.1007/s00705-019-04179-z.

[57] R. Monti, J. Contiero, A.J. Goulart, Isolation of natural inhibitors of papain obtained from Carica papaya latex, Brazil. Arch. Biol. Technol. 47 (5) (2004) 747–754, https://doi.org/10.1590/S1516-89132004000500010.

[58] P. Senthilvel, P. Lavanya, K.M. Kumar, R. Swetha, P. Anitha, S. Bag, S. Sarveswari, V. Vijayakumar, S. Ramaiah, A. Anbarasu, Flavonoid from Carica papaya inhibits NS2B-NS3 protease and prevents Dengue 2 viral assembly, Bioinformation 9 (18) (2013) 889–895, https://doi.org/10.6026/97320630009889.

[59] L.R.F. De Sousa, H. Wu, L. Nebo, J.B. Fernandes, M.F.D.G.F. Da Silva, W. Kiefer, M. Kanitz, J. Bodem, W.E. Diederich, T. Schirmeister, P.C. Vieira, Flavonoids as noncompetitive inhibitors of Dengue virus NS2B-NS3 protease: inhibition kinetics and docking studies, Bioorg. Med. Chem. 23 (3) (2015) 466–470, https://doi.org/10.1016/j.bmc.2014.12.015.

[60] B.K. Yap, C.Y. Lee, S.B. Choi, E.E. Kamarulzaman, M. Hariono, H.A. Wahab, In silico identification of novel inhibitors. Encyclopedia of Bioinformatics and Computational Biology: ABC of Bioinformatics, 1–3, 761–779. 10.1016/B978-0-12-809633-8.20158-1.

[61] S.N. Sulaiman, M. Hariono, H.M. Salleh, S.L. Chong, L.S. Yee, A. Zahari, H.A. Wahab, S. Derbré, K. Awang, Chemical constituents from Endiandra kingiana (lauraceae) as potential inhibitors for dengue Type 2 NS2B/NS3 serine protease and its molecular docking, Nat. Prod. Commun. 14 (9) (2019), https://doi.org/10.1177/1934578X19861014.

[62] M. Hariono, R. Rollando, J. Karamoy, P. Hariyono, M. Atmono, M. Djohan, W. Wiwy, R. Nuwarda, C. Kurniawan, N. Salin, H. Wahab, Bioguided fractionation of local plants against matrix metalloproteinase9 and its cytotoxicity against breast cancer cell models: in silico and in vitro study, Molecules 25 (20) (2020) 1–17, https://doi.org/10.3390/molecules25204691.

[63] M. Hariono, R.F. Nuwarda, M. Yusuf, R. Rollando, R.I. Jenie, B. Al-Najjar, J. Julianus, K.C. Putra, E.S. Nugroho, Y.K. Wisnumurti, S.P. Dewa, B.W. Jati, R. Tiara, R.D. Ramadani, L. Qodria, H.A. Wahab, Arylamide as potential selective inhibitor for matrix metalloproteinase 9 (MMP9): design, synthesis, biological evaluation, and molecular modeling, J. Chem. Inf. Model. 60 (1) (2020) 349–359.

[64] J.C. Kotta, A.B.S. Lestari, D.S. Candrasari, M. Hariono, 2020. Medicinal effect, in silico bioactivity prediction, and pharmaceutical formulation of Ageratum conyzoides L.: a review. Scientifica, 2020. 10.1155/2020/6420909.